J. Fluid Mech. (2008), *vol.* 604, *pp.* 263–296.
doi:10.1017/S0022112008001171 Printed in the United Kingdom

Can bottom friction suppress 'freak wave' formation?

VIACHESLAV V. VORONOVICH[1], VICTOR I. SHRIRA[2] AND GARETH THOMAS[1]

[1]School of Mathematics, University College Cork, Cork, Ireland
[2]Department of Mathematics, Keele University, Keele, ST5 5BG UK

(Received 31 August 2007 and in revised from 21 February 2008)

The paper examines the effect of the bottom stress on the weakly nonlinear evolution of a narrow-band wave field, as a potential mechanism of suppression of 'freak' wave formation in water of moderate depth. Relying upon established experimental studies the bottom stress is modelled by the quadratic drag law with an amplitude/bottom roughness-dependent drag coefficient. The asymptotic analysis yields Davey–Stewartson-type equations with an added nonlinear complex friction term in the envelope equation. The friction leads to a power-law decay of the spatially uniform wave amplitude. It also affects the modulational (Benjamin–Feir) instability, e.g. alters the growth rates of sideband perturbations and the boundaries of the linearized stability domains in the modulation wavevector space. Moreover, the instability occurs only if the amplitude of the background wave exceeds a certain threshold. Since the friction is nonlinear and increases with wave amplitude, its effect on the formation of nonlinear patterns is more dramatic. Numerical experiments show that even when the friction is small compared to the nonlinear term, it hampers formation of the Akhmediev/Ma-type breathers (believed to be weakly nonlinear 'prototypes' of freak waves) at the nonlinear stage of instability. The specific predictions for a particular location depend on the bottom roughness k_s in addition to the water depth and wave field characteristics.

1. Introduction

Anomalously high ocean waves, exceeding 2.3 times the significant wave height H_s and commonly referred to as 'freak' or 'rogue' waves, have been a subject of marine folklore for centuries. In recent years well-documented observations of freak wave events have become available, such as those of Haver (2000). Freak waves are often unusually steep ('walls of water'), asymmetric and short-lived, the typical event duration being of the order of just 10 wave periods. They are often preceded and/or followed by deep troughs ('holes in the sea') and may appear as a single or a group of a few successive waves ('three sisters'). But the most mysterious feature making freak waves a serious threat for navigation and offshore activities is their propensity to appear seemingly out of nowhere, i.e. in otherwise totally benign conditions and without any precursors. Starting with the pioneering work of Smith (1976), the research community has made substantial efforts to discover the mechanisms behind these rare, but unfortunately not negligibly rare, events. Considerable progress has been made, and, in the absence of wave–current interaction, two main generic mechanisms were identified: the Benjamin–Feir (BF) or modulational instability

(Peregrine 1983; Osborne, Onorato & Serio 2000), and the essentially linear space–time focusing (see e.g. Slunyaev *et al.* 2002; Kharif & Pelinovsky 2003, for a recent review). A combination of both mechanisms should be regarded as the general case.

Although observations suggest that a freak wave is typically an essentially nonlinear phenomenon, linear and weakly nonlinear mechanisms do lead to its formation, even if they cannot explain some strongly nonlinear features. The situation closely resembles that of wave breaking that in itself is an essentially nonlinear phenomenon, but is triggered by the development of some linear and weakly nonlinear effects (Song & Banner 2002). The key role of the modulational instability in the formation of freak waves is supported by the numerical experiments of Tanaka (1990) and Dyachenko & Zakharov (2005) and field observations. Janssen (2003) has introduced the *Benjamin-Feir Index* (BFI) to characterize the narrowness of the wind wave spectra (more precisely the ratio of nonlinear and dispersion effects for narrow-band spectra) and to identify those situations where the BF instability is more likely. The recorded observations of freak waves do indeed cluster around such situations.

The basic model for a deterministic description of narrow-band wave fields is the classic nonlinear Schrödinger (NLS) equation (e.g. Mei, Stiassnie & Yue 2005), which is exactly solvable (Zakharov & Shabat 1971). Some of its exact solutions appear to be plausible weakly nonlinear 'prototypes' of freak waves. These are the well-known breathers (see e.g. Dysthe & Trulsen 1999), which can be space- or time-periodic (the Akhmediev and Ma breathers respectively), or non-periodic (the Peregrine soliton); all have amplitudes exceeding the freak wave threshold. The Peregrine (1983) solution represents a limiting configuration of both the Ma and Akhmediev periodic patterns and seems to be the most plausible candidate. The hump in the envelope amplitude reaches three times the background amplitude, it appears out of nowhere and disappears without a trace. Osborne *et al.* (2000) developed a way of predicting such patterns corresponding to particular homoclinic orbits by means of an analysis of the initial data; their approach was later refined and successfully extended beyond the simple integrable model to more realistic ones by Onorato *et al.* (2001).

Compared to the amount of effort and resources spent on addressing the question of *what creates freak waves*, surprisingly little attention has been paid to another at least as important question: *What can prevent the formation of freak waves?* Indeed, what the end users, such as mariners and offshore industry, would ultimately like to know is: *Are there areas of world ocean safe from freak waves, and, if yes, where are they*?

The prime purpose of this study is to demonstrate that there exists one mechanism, namely the bottom friction, which may be sufficiently strong to arrest or totally suppress the development of freak waves. We are interested in waves in water of moderate depth, or more precisely, in the seemingly narrow range of water depth h' in terms of dominant wave wavenumber k', namely, $k'h' \sim 0.7 - 1.7$ (Throughout the paper a prime denotes dimensional variables.). A disproportional share of sea traffic and offshore activities occurs in such wave regimes. For an ocean swell of wavelength $\lambda \sim 500\,\mathrm{m}$, this corresponds approximately to the depth range $100 - 150$ m. Note that the lower boundary of the BF instability interval, $k'h' \geqslant 1.363$, applies to longitudinal instability only and the oblique one exists down to $k'h' \simeq 0.38$ as shown by Benney & Roskes (1969). The bottom friction has been so far neglected in this context, and even for water of moderate depth, it is very weak due to the nearly exponential decrease of orbital velocities with depth. The central finding of this study is that even a very weak

bottom friction can hamper the BF instability and partially or completely suppress the formation of any patterns resembling freak waves.

This paper is the first attempt to study and quantify the effect of bottom friction on the development of the BF instability and, ultimately, to address the practical questions raised above. It is known that only narrow-band wave fields can experience the modulational instability, and we restrict ourselves to the simplest possible (NLS-type) model, i.e. study the deterministic evolution of a narrow-band weakly nonlinear wave field in water of moderate constant depth. The problem statement, scaling and the asymptotic procedure are discussed in § 2. This is followed by a brief discussion of the possible flow regimes in the wave bottom boundary layer and the corresponding models of bottom stress in § 3. An asymptotic analysis is outlined in § 4 and leads to a closed set of equations, differing from the Davey & Stewartson (1974) system by the presence of bottom stress terms. It is important to note that the bottom friction results in a nonlinear term in the amplitude equation that increases with the wave amplitude. Its effect differs qualitatively from that of a linear damping of different physical origin studied by Segur *et al.* (2005), Mei & Hancock (2003) and other authors. In § 5 an examination of the linear stability of a uniform wavetrain yields the threshold value of the friction sufficient to prevent completely the BF instability. The effect of an even weaker friction on the formation of nonlinear patterns is studied in § 6. Results, along with some quantitative estimates, are discussed in § 7.

2. The problem, scaling and basic assumptions

Since only narrow-band wave fields can experience the modulational instability as discussed by Janssen (2004), we consider the simplest generic model of such a wave field; this is an arbitrary narrow-banded distribution of free water waves propagating in water of moderate constant depth. Although the analysis is valid both for ocean swell and wind waves we neglect the effect of wind at this stage. The relevance of the model for real situations and in particular, the effect of wind, will be discussed in § 7.

Choose a coordinate system with x-axis aligned with the wave vector of the carrier wave, z-axis directed vertically upward and unperturbed water surface placed at the level $z = 0$. By introducing the characteristic wave scales of length, phase speed and frequency

$$\mathscr{K} = \frac{2\pi}{\lambda}, \qquad \mathscr{C} = \left(\frac{g'}{\mathscr{K}}\right)^{1/2}, \qquad \Omega' = (g'\mathscr{K})^{1/2}, \tag{2.1}$$

the variables are made non-dimensional by

$$\left.\begin{aligned} \boldsymbol{u}' &= \mathscr{C}\boldsymbol{u}, \quad p' = \rho'\mathscr{C}^2 p, \quad \zeta = \mathscr{K}\zeta', \quad h = \mathscr{K}h', \\ \boldsymbol{r} &= \mathscr{K}\boldsymbol{r}', \quad t = \Omega' t', \qquad \omega' = \Omega'\omega, \quad k' = \mathscr{K}k. \end{aligned}\right\} \tag{2.2}$$

Here g' is the acceleration due to gravity, λ and $\mathscr{K}$ are (dimensional) wavelength and wavenumber, $\boldsymbol{u} = \{u, v, w\}$, p, ζ denote velocity, pressure and surface elevation respectively; t, $\boldsymbol{r} = \{x, y, z\}$, ω, k, h are time, position vector, frequency, wavenumber and depth, respectively. The density of the fluid ρ' is assumed to be constant. Hereinafter the dimensional variables are denoted either by primes or by script capitals. For a few dimensional variables which do not have non-dimensional counterparts throughout the paper the primes will be omitted and the fact that the variable is dimensional will be explicitly stated in the text.

The non-dimensional equations governing fluid motion are written in the form

$$\boldsymbol{q}_t + \nabla_\perp p = -(\boldsymbol{u}\cdot\nabla)\,\boldsymbol{q} + \frac{\tau_s}{\rho'\mathscr{C}^2}\frac{\partial \boldsymbol{\tau}}{\partial z}, \tag{2.3a}$$

$$w_t + (p+gz)_z = -(\boldsymbol{u}\cdot\nabla)\,w + \frac{\tau_s}{\rho'\mathscr{C}^2}\,\nabla_\perp\cdot\boldsymbol{\tau}, \tag{2.3b}$$

$$\nabla_\perp\cdot\boldsymbol{q} + w_z = 0, \tag{2.3c}$$

where

$$\nabla_\perp = \left\{\frac{\partial}{\partial x}, \frac{\partial}{\partial y}\right\}, \qquad \nabla = \left\{\frac{\partial}{\partial x}, \frac{\partial}{\partial y}, \frac{\partial}{\partial z}\right\} \tag{2.4}$$

are operators of the horizontal and full gradient, $\boldsymbol{q} = \{u, v\}$ is horizontal velocity,

$$g = \frac{g'\mathscr{K}}{\Omega'^2} \tag{2.5}$$

is the non-dimensional gravitational acceleration and

$$\boldsymbol{\tau} = \{\tau_{xz}, \tau_{yz}\} \tag{2.6}$$

is the vector of vertical stress and τ_s is its magnitude.

The standard kinematic and dynamic conditions are imposed at the moving surface of the fluid $z = \zeta$,

$$\zeta_t - w + (\boldsymbol{q}\cdot\nabla_\perp)\zeta = 0, \tag{2.7a}$$

$$p - gz = p_a, \tag{2.7b}$$

where p_a is the atmospheric pressure and at the bed

$$\boldsymbol{u} = 0 \qquad \text{at} \quad z = -h. \tag{2.7c}$$

The solution to (2.3), (2.7) is sought in the form of series

$$\begin{pmatrix} \boldsymbol{u} \\ \zeta \\ p - p_a \end{pmatrix} = \sum_{n=1}^{\infty} \varepsilon^n \sum_{m=-n}^{n} \begin{pmatrix} \boldsymbol{u}_{nm} \\ \zeta_{nm} \\ p_{nm} \end{pmatrix} \exp\{\mathrm{i}m\Theta\} \tag{2.8a}$$

in wave steepness

$$\varepsilon = \mathscr{K}\zeta_s. \tag{2.8b}$$

Here ζ_s is a typical dimensional wave height and

$$\Theta = kx - \omega t \tag{2.8c}$$

is the carrier wave phase. Since the wave fields are real functions, the amplitudes f_{nm} in (2.8) satisfy the relation

$$f_{n,-m} = \bar{f}_{nm},$$

where the overbar denotes the complex conjugate. The amplitudes are allowed to evolve at slow time and space scales

$$\left.\begin{aligned} x_1 &= \varepsilon x, \quad x_2 = \varepsilon^2 x, \quad \ldots, \\ y_1 &= \varepsilon y, \quad y_2 = \varepsilon^2 y, \quad \ldots, \\ t_1 &= \varepsilon t, \quad t_2 = \varepsilon^2 t, \quad \ldots, \end{aligned}\right\} \tag{2.9}$$

with the operators of horizontal gradient and time derivative redefined accordingly:

$$\nabla_\perp = \left\{ k\frac{\partial}{\partial\Theta}, 0 \right\} + \varepsilon\nabla_1 + \varepsilon^2\nabla_2 + \cdots, \tag{2.10a}$$

$$\frac{\partial}{\partial t} = -\omega\frac{\partial}{\partial\Theta} + \varepsilon\frac{\partial}{\partial t_1} + \varepsilon^2\frac{\partial}{\partial t_2} + \cdots. \tag{2.10b}$$

We assume that:

(*a*) The atmospheric pressure is constant and the wind stress negligible at the fluid surface, i.e.

$$p_a = \text{const}, \qquad \boldsymbol{\tau} = 0 \qquad \text{at} \quad z = \zeta. \tag{2.11}$$

Momentum exchange between the ocean and the atmosphere is known to be most effective at spatial scales much smaller than those of interest here and is almost non-existent for the developed waves at the spectral peak. The indirect transfer of momentum from wind to smaller scales and then via nonlinear interactions to the dominant waves is not explicitly taken into account either (see discussion in § 7).

(*b*) The water is stipulated to be of moderate depth:

$$kh \sim 1. \tag{2.12}$$

(*c*) The wave steepness ε deemed to be sufficiently small so that

$$\varepsilon \ll 1. \tag{2.13}$$

(*d*) The $O(\varepsilon)$ motions at the zeroth harmonic are absent, i.e.

$$\boldsymbol{u}_{10} \equiv 0, \qquad p_{10} \equiv 0, \qquad \zeta_{10} \equiv 0. \tag{2.14}$$

Equations (2.3), (2.7) do admit solutions at zeroth harmonic at $O(\varepsilon)$ but these are not induced by waves; chosen to be zero initially, they remain at most $O(\varepsilon^2)$.

The magnitude of the stress terms and their functional dependence on the wave parameters remain to be discussed. For the moment we assume that to the main order in ε the motion is unaffected by the stress, and the (1, 1) solution, i.e. the terms with $n = 1$, $m = 1$ in the series (2.8), is the usual inviscid, plane, harmonic wave of amplitude A described by

$$\left.\begin{aligned} &\zeta_{11} = A, && p_{11} = A\,\frac{\omega^2}{k}\,\frac{\cosh k(z+h)}{\sinh kh}, \\ &w_{11} = -\mathrm{i}\omega A\,\frac{\sinh k(z+h)}{\sinh kh}, && u_{11} = \omega A\,\frac{\cosh k(z+h)}{\sinh kh}, \end{aligned}\right\} \tag{2.15}$$

where the frequency and the wavenumber are connected by the linear dispersion relation

$$\omega^2 = gk\tanh kh. \tag{2.16}$$

Clearly, the no-slip condition (2.7*c*) is not satisfied by (2.15), meaning that a boundary layer of width δ' is formed near the bottom. The velocity shear inside the boundary layer is much higher than in the bulk flow and may produce significant levels of turbulence and bottom stress.

No *a priori* assumption is made concerning irrotationality of flow, in contrast to the classical studies of wave modulations in water of intermediate depth, such as those of Benney & Roskes (1969), Davey & Stewartson (1974), Djordjevic & Redekopp (1977), Mei *et al.* (2005). Indeed, the stress, however small, introduces vorticity into the flow and thus the potential approximation breaks down (Lamb 1932).

3. The stress terms and the bottom boundary layer

A wave propagating in the ocean experiences the action of two fundamental dissipative mechanisms, molecular viscosity and turbulence, which both contribute to the stress terms in (2.3). The kinematic viscosity ν_e' of seawater is $\sim 10^{-6}\,\mathrm{m^2\,s^{-1}}$ and the Reynolds number

$$Re = \frac{\mathscr{C}\lambda}{\nu_e'},$$

based on the phase speed $\mathscr{C}$ and the (dimensional) wavelength λ of swell or dominant wind waves is normally so large (of order of 10^{10}), that the influence of molecular viscosity may be safely neglected in the bulk of the fluid. It is known as well that the velocity shear produced by a wave in the body of the fluid is too weak to generate significant levels of turbulence in the absence of wave breaking or significant wind stress. A typical value of the dimensional friction velocity u_*,

$$u_*{}^2 = \frac{\tau_s}{\rho'}, \tag{3.1}$$

is of the order of $1\,\mathrm{cm\,s^{-1}}$ near the sea surface, which leads to an estimate

$$\frac{\tau_s}{\rho'\mathscr{C}^2} = \left(\frac{u_*}{\mathscr{C}}\right)^2 \sim 10^{-7}, \tag{3.2}$$

which indicates that the turbulent stresses are negligibly weak in the bulk of the water. The solution of (2.3) is essentially inviscid away from the bottom. There is always a well-developed surface turbulent boundary layer (Terray *et al.* 1996). However, the dissipation experienced by the dominant wave is mainly due to the formation of a bottom boundary layer (BBL), where the velocity shear is much stronger and a significant amount of turbulence may be generated.

The nature of the BBL and the structure of the flow therein depend strongly on whether the BBL should be considered steady or oscillatory (OBL). The boundary layers that can be treated as steady, such as those associated with tidal currents, have much greater thickness and often extend well into the bulk of fluid, while the velocity variation with the distance from the bottom follows the well-known 'law of the wall' described by Soulsby (1990). On the contrary, an OBL is created and destroyed at every wave period; its width δ' is usually very small in comparison to the total depth and varies with time; the velocity within often does not follow the log-law as demonstrated Kajiura (1968) and Jensen, Sumer & Fredsøe (1989). A criterion *a priori* separating these two types of flow was proposed by Kajiura (1964), who considered the relative importance of the pressure gradient and the inertia in the BBL. According to Kajiura, for motion of frequency ω' in water of depth h', the BBL is oscillatory, provided

$$\frac{\mathscr{U}}{\omega' h'} \lesssim 40, \tag{3.3}$$

where $\mathscr{U}$ is the magnitude of orbital velocity at the outer border of the BBL.

Solution (2.8) is composed of multiple harmonics of the fundamental frequency ω plus a slowly evolving induced current. It is natural to assume that the bottom stress will exhibit the same structure, i.e. may be represented as a series

$$\boldsymbol{\tau} = \sum_{-\infty}^{\infty} \hat{\boldsymbol{\tau}}^{(m)} \exp\{\mathrm{i}m\Theta\}, \tag{3.4}$$

	ε	λ (m)	$\mathscr{K}$ (m^{-1})	$\mathscr{C}$ ($m\,s^{-1}$)	Ω' (s)	ζ_s (m)
Case A (swell)	0.05	500	0.0126	27.9	0.35	4
Case B (wind waves)	0.1	100	0.0628	12.5	0.79	1.6

TABLE 1. Values of the wave parameters chosen for estimates.

where $\hat{\boldsymbol{\tau}}^{(m)}$ do not depend on the fast variables, as proposed by Jonsson (1980). Each harmonic in the expansion (2.3) creates its own boundary layer near the bottom. Obviously, these are overlapping and therefore inter-harmonic interaction may occur. However, we assume that this interaction may be neglected and each term in (3.4) is dealt with separately. In particular, the magnitude, phase and vertical distribution of $\hat{\boldsymbol{\tau}}^{(m)}$ are assumed to be independent of the parameters, such as orbital velocity and excursion, of harmonics other than the mth.

This is a rather bold assumption, since there exists a considerable amount of data suggesting the opposite. In particular, wave interaction with a steady current in the near-bed region has attracted considerable attention, for example Soulsby *et al.* (1993). It has been found that the effect of waves does change the current's BL, since waves effectively create an additional roughness at the bottom, which leads to an increase of the bottom stress experienced by the current (Grant & Madsen 1979). However, no reverse influence has been discovered, even when the velocities induced by the current exceed those induced by the waves by several times (Nielsen 1992). A plausible explanation is that the width of the wave boundary layer (WBL) is much smaller than that of the current and hence the velocity gradients within the wave BBL are orders of magnitude larger. Little is known about the interaction between two oscillating flows; however, one should take into account the property that the velocities at the bottom associated with higher harmonics are much smaller than at the fundamental frequency, due to both the amplitude scaling (2.8*a*) and faster decay of the velocity with depth. Thus, to leading order, the only interaction effect that has to be taken into account is the action of the fundamental harmonic on the induced flow.

Let us choose for the estimates two sets of wave parameters corresponding to typical swell and wind waves, denoted by Case A and Case B and presented in table 1. In both cases we set

$$h = 1.5, \qquad k = 1, \qquad \omega = \tanh kh \tag{3.5}$$

corresponding to water of depths $h' \approx 120\,\mathrm{m}$ and $h' \approx 25\,\mathrm{m}$, respectively. The magnitudes of orbital velocity $\mathscr{U}$ and excursion of a fluid particle $\mathscr{A}$ near the bottom, at the first harmonic, can be calculated from (2.15)

$$\mathscr{U} = \frac{\varepsilon \mathscr{C} \omega}{\sinh kh}, \qquad \mathscr{A} = \frac{\mathscr{U}}{\omega \Omega'} = \frac{\varepsilon \mathscr{K}^{-1}}{\sinh kh}. \tag{3.6}$$

The estimate for the induced flow should take into account the property of uniformity over the entire depth (see § 4); at the same time the magnitude of its velocity is of order of $\varepsilon^2 \mathscr{C}$. Moreover, it is a motion with a much longer time scale, namely, $\varepsilon^{-1} \Omega'^{-1}$. The orbital velocity and excursion associated with the induced flow are then given by

$$\mathscr{U}^{(0)} \simeq \varepsilon^2 \mathscr{C}, \qquad \mathscr{A}^{(0)} \simeq \frac{\mathscr{U}^{(0)}}{\varepsilon\, \Omega'} \simeq \varepsilon \frac{\mathscr{C}}{\Omega'} = \varepsilon \mathscr{K}^{-1}. \tag{3.7}$$

	$\mathscr{U}$ (m s^{-1})	$\mathscr{A}$ (m)	$\mathscr{U}^{(0)}$ (m s^{-1})	$\mathscr{A}^{(0)}$ (m)
Case A (swell)	0.62	1.87	0.07	3.98
Case B (wind waves)	0.56	0.75	0.12	1.59

TABLE 2. Orbital velocities for excursions near the bed.

	Re_a	Ro	$Re_a^{(0)}$	$Ro(0)$
Case A (swell)	1.1×10^6	37	2.5×10^5	79
Case B (wind waves)	3.8×10^6	15	1.8×10^5	32

TABLE 3. Reynolds and roughness numbers.

The quantitative estimates corresponding to Cases A and B are given in table 2. Substituting the values of $\mathscr{U}$, $\mathscr{U}^{(0)}$ obtained for Case A into Kajiura's criterion gives

$$\frac{\mathscr{U}}{\omega' h'} \approx 0.016, \qquad \frac{\mathscr{U}^{(0)}}{\omega'^{(0)} h'} \simeq \frac{\varepsilon \mathscr{C}}{\Omega' h'} \approx 0.033, \tag{3.8}$$

and suggests that the boundary layers at both the fundamental and zeroth-harmonic should be treated as oscillatory. The corresponding values for Case B are 0.03 and 0.061 respectively and the conclusion remains the same for the whole range of wave scales and parameters that might be of interest in the context of freak waves.

The flow in the OBL is mainly controlled by two non-dimensional parameters, the amplitude Reynolds number Re_a and the roughness number Ro, defined by

$$Re_a = \frac{\mathscr{U}\mathscr{A}}{\nu_e}, \qquad Ro = \frac{\mathscr{A}}{k_s}, \tag{3.9}$$

where k_s is the dimensional Nikuradze roughness of the bottom (Soulsby 1998). Taking the conservative estimate $k_s \simeq 5\,\mathrm{cm}$ yields the set of values found in table 3.

Nielsen (1992) and Soulsby (1998), and references therein, suggest that the values in table 3 correspond to boundary layers that are '*rough turbulent*' both at the first and zeroth harmonic and for both the swell and the wind waves. In a rough-turbulent OBL the dependence of the properties of the flow on Re_a is completely lost and the roughness number Ro remains the only governing parameter. Numerous attempts to build an analytical model of a turbulent OBL have been made, mainly using the concept of eddy viscosity. Within the framework of such an approach, the turbulent stress in the OBL is presented in the form

$$\boldsymbol{\tau} = \nu_t \frac{\partial \boldsymbol{u}}{\partial z}, \tag{3.10}$$

where ν_t is the eddy viscosity, either constant through the BL or, more often, depth-dependent. The usual approach is to solve the equations of motion in the BL and to match the solution to the inviscid flow. There are some complete flow models, such as that presented by Thais *et al.* (2001). However this common approach has serious disadvantages. Experiments suggest that the log-layer is absent at roughness numbers Ro smaller than 50, and even at larger values it appears only at certain phases of the flow. This renders dimensional analysis, similar to that used in steady BLs, void and requires a prescription of ν_t as a function of z from the very beginning in a somewhat arbitrary way. In the OBL ν_t may also be time-dependent and complex, which makes

the equations obtained more difficult to solve (see Nielsen 1992). More importantly, the experiments of Sleath (1987) clearly show that the total stress in the OBL is an order of magnitude larger than that caused by turbulence proper. This is due to the fact that the flow in the boundary layer is non-potential and the wave-induced stress $\tau_w = \rho' \widetilde{\tilde{u}\tilde{w}}$ is non-zero and large (Nielsen 1992). All in all, using the concept of eddy viscosity in oscillatory flow is not well justified and does not appear to provide any advantage over much simpler models, such as based on wave drag, unless one is interested in the OBL inner structure itself.

The dimensional analysis of Soulsby (1990) suggests that the thickness of the turbulent boundary layer is inversely proportional to the frequency of the flow,

$$\delta' \sim \frac{u_*}{\omega'}, \tag{3.11}$$

where u_* is the friction velocity in the BBL. This result is well corroborated by the experimental data of Klopman (1994). Taking $u_* \approx 3\,\mathrm{cm\,s^{-1}}$, the dimensional boundary layer thickness δ' is estimated to be a few tens of centimetres and the non-dimensional

$$\delta = \mathscr{K}\delta' \simeq 5 \times 10^{-4}.$$

Within this very thin layer the flow is almost horizontal, with velocity and stress varying rapidly and the magnitude of the stress falling almost to zero at the height of a few multiples of δ' from the bottom (Jonsson 1980). In our context, fortunately, the internal structure and dynamics of the BBL can be ignored; it is natural to assume that all the stress is applied at a point $z = -h$. To describe this stress we adopt a drag law, similar to that used by hydraulic engineers:

$$\frac{\boldsymbol{\tau}'}{\rho'} = \frac{f_w}{2} |\boldsymbol{U}| \boldsymbol{U} \tag{3.12}$$

where f_w is called the friction coefficient. Note two principal differences from the standard steady case:

(*a*) There exists a phase lag, φ, between the stress and the orbital velocity, so that

$$\hat{\boldsymbol{\tau}}^{(m)} = |\hat{\boldsymbol{\tau}}^{(m)}| \mathrm{e}^{\mathrm{i}\varphi_m} \tag{3.13}$$

The value of the phase lag in a laminar OBL (Stokes layer) is well known, $\varphi_\lambda = 45°$, but no reliable theoretical estimate exists for the turbulent one. The experimental data suggest the value

$$\varphi \approx 25° - 30° \tag{3.14}$$

at $15 \lesssim Ro \lesssim 70$ (Jonsson 1980; Jensen *et al.* 1989; Nielsen 1992).

(*b*) In a rough-turbulent OBL, f_w is not a universal constant but a function of the roughness number Ro. Several models of this dependence have been proposed by Swart (1974), Myrhaug (1989) and others. However, the model of Soulsby (1998) seems to be the simplest, most robust and the most suitable for our purposes. It suggests a polynomial law

$$f_w = 0.237 Ro^{-\sigma}, \tag{3.15}$$

with an exponent $\sigma \approx 0.52$, obtained by the fit to a large set of experimental data (see figure 1) taken from seven different sources as detailed in figure 9 of Soulsby *et al.* (1993).

Substituting the wave parameters and estimates of orbital velocities given into (3.12) results in the values of the friction coefficients and stress magnitudes given in table 4.

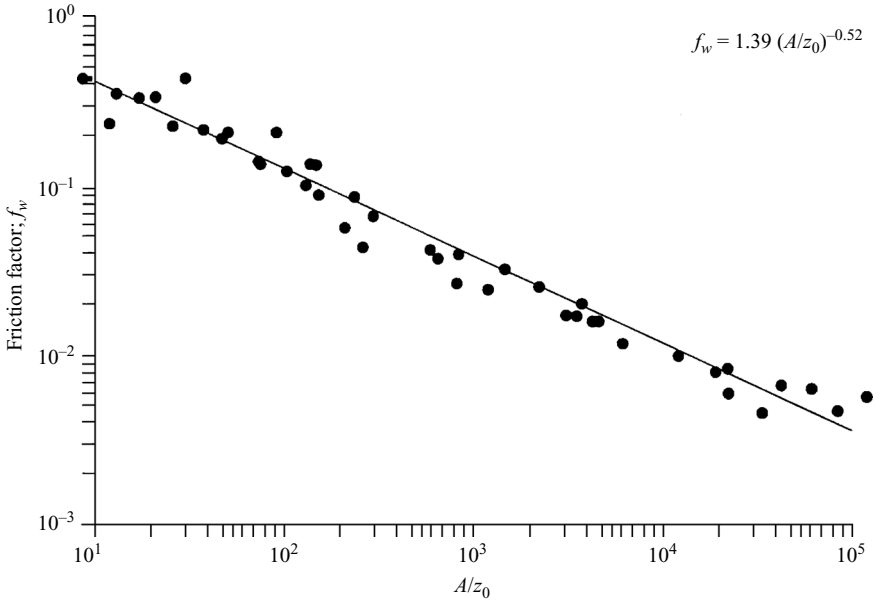

FIGURE 1. Dependence of the friction coefficient, f_w on the roughness number Ro. (Based on Soulsby (1998), figure 15.)

	$f_w^{(1)}$	$\tau_s^{(1)}\rho_*^{-1}$ (m^2 s^2)	$f_w^{(0)}$	$\tau_s^{(0)}\rho_*^{-1}$ (m^2 s^2)
Case A (swell)	0.036	7.02×10^{-3}	0.024	5.9×10^{-5}
Case B (wind waves)	0.058	9.05×10^{-3}	0.039	3.06×10^{-4}

TABLE 4. Values of the friction coefficient and bottom stress at the first and zeroth harmonic.

The stress experienced by the induced flow proves to be one or two orders of magnitude smaller than that at the fundamental frequency. It is also clear that the bottom stress acting on the higher harmonics is negligible, since the corresponding orbital velocities are orders of magnitude smaller than at the fundamental frequency. We therefore set

$$\hat{\boldsymbol{\tau}}^{(m)} = 0, \qquad \forall\, m \neq 1 \tag{3.16a}$$

in what follows.

We further infer that the effect of the bottom stress is exhibited at the same order as nonlinearity/wave modulations, i.e. at ε^3, and write the stress term at the fundamental frequency in (2.3) in the form

$$\frac{\tau_s^{(1)}}{\rho' \mathscr{C}^2}\,\tau_{xz}^{(1)} = \varepsilon^3 \hat{\tau} \mathrm{e}^{\mathrm{i}\Theta}, \tag{3.16b}$$

where the non-dimensional stress $\hat{\tau}(z)$ is non-zero only within the BBL, i.e. at

$$-h < z \lesssim -h + \delta. \tag{3.16c}$$

The value of the stress at the bottom is derived from the drag law (3.12), (3.15)

$$\hat{\tau}\big|_{-h} = \hat{\tau}_b = \tilde{\nu} \exp\{\mathrm{i}\varphi\}\, |A|^{1-\sigma} A, \tag{3.16d}$$

with the friction coefficient $\tilde{\nu}$ given by

$$\tilde{\nu} = \varepsilon^{-3}\frac{\tau_s^{(1)}}{\rho' C^2} = 0.1185\,\varepsilon^{-3}\left(\frac{\varepsilon \mathscr{K}^{-1}}{k_s \sinh kh}\right)^{-\sigma}\left(\frac{\varepsilon\,\omega}{\sinh kh}\right)^2$$
$$= 0.237\left(\frac{1}{\varepsilon}\right)^{1+\sigma}\left(\mathscr{K} k_s\right)^{\sigma}\frac{\sinh^{\sigma} kh}{\sinh 2kh}. \tag{3.16e}$$

The spanwise component of the stress is obviously zero since in our case the carrier wave is plane and the orbital velocity is collinear with the wave vector.

4. The evolution equations

The novel feature of the analysis to follow is an attempt to take into account and quantify the effect of the bottom stress on the wave modulations. Apart from the necessity of dealing with the stress terms, the analysis follows a route originating from the classical papers of Benney & Roskes (1969) and Davey & Stewartson (1974). For example, to obtain the second-order corrections to the velocity, surface elevation and pressure fields one has to substitute the solutions (2.15) into the equations and boundary conditions, then collect the terms at zero, first and second harmonics separately and solve the equations obtained. The corrections to the first, the zeroth and the second harmonic are then used in a similar way to proceed to $O(\varepsilon^3)$. For brevity we omit certain standard steps, not essential for the main goal. These are readily available in the literature, for example Colin, Dias & Ghidaglia (1995), who used a very similar approach not relying upon the assumption of the potentiality of the motion, but did not take account of friction.

The calculations for the first harmonic at $O(\varepsilon^2)$ lead to the standard transport equation for the wave envelope

$$A_{t_1} + c_g A_{x_1} = 0, \tag{4.1a}$$

where c_g is the group speed of the carrier given by

$$c_g = \frac{\omega}{k}\left(\frac{1}{2} + \frac{kh}{\sinh 2kh}\right). \tag{4.1b}$$

The induced flow (zeroth harmonic) manifests itself at this order through an additional, depth-independent, pressure field P,

$$p_{20} = P - \omega^2|A|^2\frac{\cosh 2k(z+h)}{\sinh^2 kh}, \qquad P_z \equiv 0, \tag{4.2a}$$

a setup/setdown

$$g\zeta_{20} = P - \frac{\omega^2|A|^2}{\sinh^2 kh} \tag{4.2b}$$

and a purely horizontal velocity field

$$\boldsymbol{u}_{20} = \{\boldsymbol{q}_{20}, 0\}. \tag{4.2c}$$

None of the fields associated with the induced flow can be found at this order.

4.1. $O(\varepsilon^3)$: *zeroth harmonic*

According to our estimates in § 3, the bottom stress for the zeroth harmonic is negligible and does not affect the induced flow. Thus straightforward algebra leads

to the following set of equations:

$$\frac{\partial \boldsymbol{q}_{20}}{\partial t_1} + \nabla_1 P = 0, \tag{4.3a}$$

$$\nabla_1 \cdot q_{20} + \frac{\partial w_{30}}{\partial z} = 0, \tag{4.3b}$$

$$\frac{\partial \zeta_{20}}{\partial t_1} + 2\omega \coth kh \, \frac{\partial |A|^2}{\partial x_1} - w_{30}\big|_{z=0} = 0. \tag{4.3c}$$

The $O(\varepsilon^3)$ corrections to the pressure and the surface elevation are

$$p_{30} = \frac{\omega^2}{\sinh^2 kh} (z+h) \sinh 2k(z+h) \mathbb{N}[A], \tag{4.4a}$$

$$\zeta_{30} = 2h \, \mathbb{N}[A], \tag{4.4b}$$

where the operator $\mathbb{N}$ takes the form

$$\mathbb{N}[A] = \mathrm{i}\{\bar{A} A_{x_1} - A \bar{A}_{x_1}\}. \tag{4.4c}$$

Equation (4.3*a*) indicates that the velocity of the induced flow is depth-independent, except in the BBL. Integrate (4.3*b*) with respect to z from $-h$ to 0, add the result to (4.3*c*) and substitute for ζ_{20} from (4.2*b*) to obtain

$$\frac{\partial P}{\partial t_1} + g \int_{-h}^{0} \nabla_1 \cdot q_{20} \, \mathrm{d}z = \frac{\omega^2}{\sinh^2 kh} \frac{\partial |A|^2}{\partial t_1} - \frac{2g^2}{\omega} \frac{\partial |A|^2}{\partial x_1}. \tag{4.5}$$

The induced flow velocity $\boldsymbol{q}_{20}$ can now be excluded from (4.5) with the use of (4.3*a*) and the time derivative exchanged for the spatial one,

$$\frac{\partial}{\partial t_1} \to -c_g \frac{\partial}{\partial x_1}, \tag{4.6}$$

due to (4.1). A single equation for the pressure P results with a forcing determined by the wave envelope A

$$\left\{ \frac{c_g^2}{gh} \frac{\partial^2}{\partial x_1^2} - \nabla_1^2 \right\} P = \beta_p \frac{\partial^2 |A|^2}{\partial x_1^2} \tag{4.7a}$$

$$\beta_p = \frac{c_g^2 \omega^2}{gh \sinh^2 kh} \left\{ 1 + \frac{g}{c_g \omega} \sinh 2kh \right\} \tag{4.7b}$$

The equation does not contain dissipative terms and coincides with that obtained in the classical model of Davey & Stewartson (1974).

4.2. $O(\varepsilon^3)$: *first harmonic*

Equation (4.7) contains two independent variables, the envelope function A and the induced pressure P. We need an additional relation between them to close the system, which is obtained by solving the system (2.3), (2.7) for the first harmonic at $O(\varepsilon^3)$. It is at this order that the effect of the bottom stress is taken into account. Therefore, the boundary layer cannot be neglected and the induced flow velocity $\boldsymbol{q}_{20}$ cannot be considered constant down to the bed. Employing (3.16*b*), equations (2.3) can be cast

into the following form:

$$-\mathrm{i}\omega u_{31} + \mathrm{i}k p_{31} = F_h + \frac{\partial \hat{\tau}}{\partial z}, \tag{4.8a}$$

$$-\mathrm{i}\omega w_{31} + \frac{\partial p_{31}}{\partial z} = F_v + \mathrm{i}k\hat{\tau}, \tag{4.8b}$$

$$\mathrm{i}k u_{31} + \frac{\partial w_{31}}{\partial z} = F_c. \tag{4.8c}$$

Through cross-differentiation (4.8) can be reduced to a single equation for the pressure correction

$$\frac{\partial^2 p_{31}}{\partial z^2} - k^2 p_{31} = F_p + 2\mathrm{i}k\frac{\partial \hat{\tau}}{\partial z}. \tag{4.9}$$

The surface boundary conditions can be manipulated in a standard way into

$$\left(\frac{\partial p_{31}}{\partial z} - \frac{\omega^2}{g}\, p_{31}\right)_{z=0} = F_s. \tag{4.10}$$

Functions F_h, F_v, F_p, F_s depend on the wave and induced flow parameters, as well as upon the independent variables. Their explicit forms are rather cumbersome but exactly the same as in the non-dissipative case (see e.g. Colin *et al.* 1995).

Multiply (4.9) by $\cosh k(z+h)/\cosh kh$ and integrate the result over the depth. Integration by parts of the left-hand side produces

$$\int_{-h}^{0} \frac{\cosh k(z+h)}{\cosh kh}\left(\frac{\partial^2 p_{31}}{\partial z^2} - k^2 p_{31}\right)\mathrm{d}z = \left(\frac{\partial p_{31}}{\partial z} - \frac{\omega^2}{g}\, p_{31}\right)_0 - \frac{1}{\cosh kh}\left.\frac{\partial p_{31}}{\partial z}\right|_{-h}. \tag{4.11}$$

The last term can be estimated from (4.8*b*) as

$$\left.\frac{\partial p_{31}}{\partial z}\right|_{-h} = \mathrm{i}k\hat{\tau}_b, \tag{4.12}$$

since both w_{31} and F_p are exactly zero at the bottom.

Integration of the stress term on the right-hand side of (4.9) yields

$$\int_{-h}^{0} \frac{\cosh k(z+h)}{\cosh kh}\frac{\partial \hat{\tau}}{\partial z}\,\mathrm{d}z = -\frac{\hat{\tau}_b}{\cosh kh} - k\int_{-h}^{0} \frac{\sinh k(z+h)}{\cosh kh}\,\hat{\tau}\,\mathrm{d}z, \tag{4.13}$$

as the stress is absent at the surface. Since the stress is different from zero within the boundary layer only, and due to (3.16*c*), the last term on the right-hand side can be estimated as

$$k\int_{-h}^{0} \frac{\sinh k(z+h)}{\cosh kh}\,\hat{\tau}\,\mathrm{d}z \simeq \frac{k}{\cosh kh}\int_{-h}^{-h+\delta} k(z+h)\,\hat{\tau}\,\mathrm{d}z \lesssim \frac{\max\{\hat{\tau}\}}{2\cosh kh}(k\delta)^2.$$

The result is proportional to the square of the small parameter $k\delta$ and can be safely neglected.

Using (4.10)–(4.13), we arrive at the identity

$$F_s = \int_{-h}^{0} \frac{\cosh k(z+h)}{\cosh kh}\,F_p\,\mathrm{d}z - \frac{\mathrm{i}k\hat{\tau}_b}{\cosh kh}. \tag{4.14}$$

Substituting known explicit expressions for F_s, F_p into (4.14) yields the second evolution equation connecting the wave envelope A and the induced pressure P:

$$\mathrm{i}\frac{\partial A}{\partial t_2} + \frac{\omega_{kk}}{2}\frac{\partial^2 A}{\partial x_1^2} + \frac{c_g}{2k}\frac{\partial^2 A}{\partial y_1^2} + \alpha|A|^2 A - \beta_a P A + \frac{\mathrm{i}k\hat{\tau}_b}{2\omega\cosh kh} = 0 \tag{4.15a}$$

where

$$\alpha = -\frac{\omega k^2}{4}\tanh^2 kh\,(9\coth^6 kh - 12\coth^4 kh + 13\coth^2 kh - 2), \tag{4.15b}$$

$$\beta_a = \frac{\omega k}{g\sinh 2kh} + \frac{k}{c_g}. \tag{4.15c}$$

Let us introduce new independent variables

$$t = t_2, \qquad x = \left(\frac{2}{|\omega_{kk}|}\right)^{1/2} x_1, \qquad y = \left(\frac{2k}{c_g}\right)^{1/2} y_1, \tag{4.16a}$$

and new coefficients

$$\eta = 1 - \frac{c_g^2}{gh}, \qquad s = \frac{|\omega_{kk}|k}{c_g}. \tag{4.16b}$$

Taking into account that for gravity waves,

$$\eta > 0, \quad \omega_{kk} < 0, \qquad \forall\, k \tag{4.17}$$

the system (4.7), (4.15) can be rewritten in the form

$$\mathrm{i}A_t - A_{xx} + A_{yy} + \alpha|A|^2 A - \beta_a P A + \mathrm{i}\nu_* \mathrm{e}^{\mathrm{i}\varphi}|A|^{1-\sigma} A = 0, \tag{4.18a}$$

$$\left(\eta\frac{\partial^2}{\partial x^2} + s\frac{\partial^2}{\partial y^2}\right) P = -\beta_p \left(|A|^2\right)_{xx}, \tag{4.18b}$$

where

$$\nu_* = \frac{k\tilde{\nu}}{2\omega\cosh kh} = 0.059\left(\frac{1}{\varepsilon}\right)^{1+\sigma}\left(\mathscr{K}k_s\right)^{\sigma}\frac{k}{\omega}\frac{\sinh^{\sigma-1} kh}{\cosh^2 kh}, \tag{4.18c}$$

which differs from the classical Davey–Stewartson equations only by the presence of the complex nonlinear friction term.

Note that in situations where nonlinear friction affects primarily the first harmonic (as in our case), sometimes the quadratic damping term can also be treated by equivalent linearization whereby the quadratic formula is replaced by a linear formula, with the damping coefficient in the latter determined by requiring the two formulae to give the same rate of energy dissipation (see Mei *et al.* 2005, p. 285). This simplification could to some extent be justified when one is interested in the evolution of the mean amplitude of random wave fields. Here we are primarily interested in nonlinear dynamics of 'individual' patterns, where the specific form of friction could prove important. Therefore, throughout the paper we will study (4.18) preserving the nonlinear friction as it is.

Consider first for simplicity one-dimensional modulations, i.e. assume for the time being the wave amplitude not to depend on the spanwise coordinate (the two-dimensional case is considered in Appendix A). The induced flow becomes a purely forced motion

$$P_u = -\frac{\beta_p}{\eta}|A_u|^2, \tag{4.19a}$$

and the system (4.18) reduces to a self-focusing NLS equation, modified by the friction term,

$$\mathrm{i}A_t - A_{xx} + \alpha_{\parallel}|A|^2 A + \mathrm{i}\nu_* \mathrm{e}^{\mathrm{i}\varphi}\,|A|^{1-\sigma} A = 0, \tag{4.19b}$$

where

$$\alpha_{\parallel} = \alpha + \frac{\beta_a \beta_p}{\eta}. \tag{4.19c}$$

5. Linear stability

Helpful insight into the effect of friction on the modulational instability within the framework of the modified Davey–Stewartson system (4.18) is provided by the standard analysis of linear stability. Consider a uniform wavetrain with superimposed infinitesimal harmonic sidebands

$$A = A_u(1 + \hat{\varepsilon}\,\hat{a})\exp[\mathrm{i}\Theta_u], \tag{5.1a}$$

$$P = P_u + \hat{\varepsilon}\,\hat{p}, \tag{5.1b}$$

where A_u, Θ_u are functions of time only,

$$\begin{pmatrix} \hat{p} \\ \hat{a} \end{pmatrix} = \begin{pmatrix} p \\ a \end{pmatrix} \cos(mx + ly), \tag{5.1c}$$

and $\hat{\varepsilon}$ is a new formal small parameter representing the perturbation. Provided the wave vector of the sideband falls within the 'instability region' in the (m, l)-plane, the amplitudes a, p grow exponentially until slowed down and halted by nonlinearity. The whole process can be described as energy transfer from the carrier to the sidebands and back, which at the nonlinear stage of evolution can lead to the formation of nonlinear patterns such as solitary waves and breathers. The 'instability regions' are bordered by the 'soft'

$$l^2 - m^2 = 0 \tag{5.2a}$$

and 'hard', i.e. amplitude-dependent,

$$l^2 - m^2 = 2\alpha_\vartheta A_u^2 \tag{5.2b}$$

neutral stability curves (see Benney & Roskes 1969; Mei *et al.* 2005, for details). Here

$$\alpha_\vartheta = \alpha + \frac{\beta_a \beta_p}{\eta}\, f_\vartheta, \qquad\qquad f_\vartheta = \left(1 + \frac{s}{\eta}\tan^2\vartheta\right)^{-1} \tag{5.2c}$$

and ϑ is the angle at which the perturbation travels, measured from the x-axis

$$\tan\vartheta = \frac{l}{m} \tag{5.2d}$$

and s, η are given by (4.16*b*). The earlier introduced $\alpha_{\parallel}$ corresponds to the case of strictly longitudinal envelope perturbations with $\vartheta = 0$.

The effect of dissipation on the onset and development of the modulational instability has been studied extensively in different contexts, mainly on the basis of the NLS equation, and (to the best of our knowledge) only with a friction term *linear* in amplitude. This is an appropriate model for the propagation of light in lossy fibres (Hasegawa & Tai 1989; Karlsson 1995), of water waves over a random seabed (Mei & Hancock 2003) and of water waves in deep narrow channels typical

of laboratory tanks (Segur *et al.* 2005). The linear friction leads to an exponential decay of the carrier amplitude and may influence the instability in different ways.

Part of the energy of the carrier wave is lost due to friction and its amplitude decays with time. This limits the energy available for the transfer to unstable wavenumbers, decreases the growth rates and, overall, hampers the development of instability. The location of the 'hard' stability curve shifts as A_u decreases, and the instability regions shrink. A sideband that was initially unstable typically leaves the region of instability and stops growing after some time.

However, our analysis suggests that the NLS equation with linear friction is not an appropriate model for waves in water of moderate depth. The effect of induced flow is important and the principal dissipative effect, the bottom stress, is essentially *nonlinear*. Therefore, its effect on the sideband instability is expected to differ from the previous findings.

On substituting (5.1) into (4.18) and separating real and imaginary parts, at $O(1)$ we obtain (4.19*a*), plus

$$\dot{A}_u + \nu_* \cos\varphi\, A_u^{2-\sigma} = 0, \tag{5.3a}$$

$$\dot{\Theta} - \alpha_\parallel A_u^2 + \nu_* \sin\varphi\, A_u^{1-\sigma} = 0, \tag{5.3b}$$

where the dot denotes the time derivative. Introducing a new dependent variable

$$\Lambda = (1-\sigma)\,\nu_*\, \cos\varphi\, A_u^{1-\sigma}, \tag{5.4}$$

it becomes clear that (5.3*a*) implies

$$\dot{\Lambda} = -\Lambda^2, \tag{5.5}$$

which can be easily integrated

$$\Lambda = \frac{\Lambda_0}{1+\Lambda_0\, t}. \tag{5.6}$$

Thus the amplitude of the carrier does not decay exponentially, as in the case of a linear friction, but follows a power law. Obviously, the linear friction is a degenerate case corresponding to a singular limit $\sigma \to 1$. Note that if our basic state is already a nonlinear pattern, say an envelope soliton or cnoidal wave, such that to the leading order its energy is not a quadratic function of the amplitude, then its decay could be algebraic even in the case of linear damping, see e.g. Mei & Li (2004).

In the linear approximation in $\hat{\varepsilon}$, we find that $\hat{p}$ is a forced field

$$p = -\frac{\beta_p}{\eta}\, f_\vartheta\, A_u^2 (a + \bar{a}) \tag{5.7}$$

and the amplitude of the sidebands is governed by the following system of equations:

$$a_t = \mathrm{i}\left\{\mu + \alpha_\vartheta A_u^2 + \frac{\mathrm{i}}{2}\,\nu_*(1-\sigma)\,\mathrm{e}^{\mathrm{i}\varphi}\, A_u^{1-\sigma}\right\} a + \mathrm{i}\left\{\alpha_\vartheta A_u^2 + \frac{\mathrm{i}}{2}\,\nu_*(1-\sigma)\,\mathrm{e}^{\mathrm{i}\varphi}\, A_u^{1-\sigma}\right\} \bar{a}, \tag{5.8a}$$

$$\bar{a}_t = -\mathrm{i}\left\{\alpha_\vartheta A_u^2 - \frac{\mathrm{i}}{2}\,\nu_*(1-\sigma)\,\mathrm{e}^{-\mathrm{i}\varphi}\, A_u^{1-\sigma}\right\} a - \mathrm{i}\left\{\mu + \alpha_\vartheta A_u^2 - \frac{\mathrm{i}}{2}\,\nu_*(1-\sigma)\,\mathrm{e}^{-\mathrm{i}\varphi}\, A_u^{1-\sigma}\right\} \bar{a}, \tag{5.8b}$$

where a new parameter

$$\mu = m^2 - l^2 \tag{5.9}$$

is introduced to shorten the notation.

Owing to the decay of the carrier amplitude with time, the coefficients in (5.8) are time-dependent; in general, no solution can be found in closed form. This is not a major setback, however, since the linear analysis is valid only at the initial stages of the sideband evolution, when its amplitude may be considered infinitesimal.

5.1. *Growth rates, instability domains and the amplitude threshold*

Let us first study the system (5.8) at times short compared to the time scale of the carrier decay

$$0 < t \ll \left|\frac{\Lambda}{\dot{\Lambda}}\right|_0 = \Lambda_0^{-1}. \tag{5.10}$$

At this stage the decay of the carrier amplitude can be neglected and A_u, Λ could be treated as constants. Assuming

$$a(t) \sim \exp(\gamma t), \tag{5.11}$$

one immediately finds the equation for the growth rates

$$\gamma^2 + \Lambda\gamma + D = 0, \tag{5.12a}$$

where

$$D = \mu\left(\mu + 2\alpha_\vartheta A_u^2 - \tan\varphi\,\Lambda\right), \tag{5.12b}$$

and its solution in explicit form

$$\gamma = -\frac{\Lambda}{2} \pm \left[\frac{\Lambda^2}{4} - D\right]^{1/2}. \tag{5.13}$$

For instability to occur the real part of γ must be positive, which implies

$$\frac{\Lambda^2}{4} - D > \frac{\Lambda^2}{4} \qquad \Rightarrow \qquad D < 0. \tag{5.14}$$

Equation (5.14) specifies the 'instability domain' in the (m, l)-plane, once the values of the initial amplitude A_u and the friction parameters ν_*, φ are given. Figure 2 shows the instability regions for several values of the initial amplitude and ν_* in water of intermediate depth $kh = 1.5$. Hatched domains bounded by dashed curves correspond to the conservative case $\nu_* = 0$. The instability regions seem to widen with the growth of dissipation. This fact, though, is surprising only at first sight, since the sideband amplitude a_m is relative. To find the absolute values it must be multiplied by A_u, which is decreasing in time. The growth rate (5.13) is very small near the stability curves, certainly smaller than the decay rate of the carrier, $\gamma \ll \Lambda$. Thus in absolute terms, the amplitude decreases in these regions.

To check this argument let us consider the linear stability of the absolute perturbation

$$b = A_u a, \qquad \Rightarrow \quad b_t = A_u a_t + \dot{A}_u a. \tag{5.15}$$

Multiply (5.8) by A_u, and add

$$\dot{A}_u a = \frac{\dot{A}_u}{A_u}\, b = -\frac{\Lambda}{1-\sigma}\, b$$

on the right and on the left to obtain equations for b, $\bar{b}$. Look again for exponentially growing solutions, $b \sim \exp\{\gamma_{abs} t\}$. Owing to the added terms (5.13) transforms to

$$\gamma_{abs}^2 + \frac{3-\sigma}{1-\sigma}\,\Lambda\gamma_{abs} + \left\{\mu\left(\mu + 2\alpha_\vartheta A_u^2 - \Lambda\tan\varphi\right) + \frac{2-\sigma}{(1-\sigma)^2}\,\Lambda^2\right\} = 0. \tag{5.16}$$

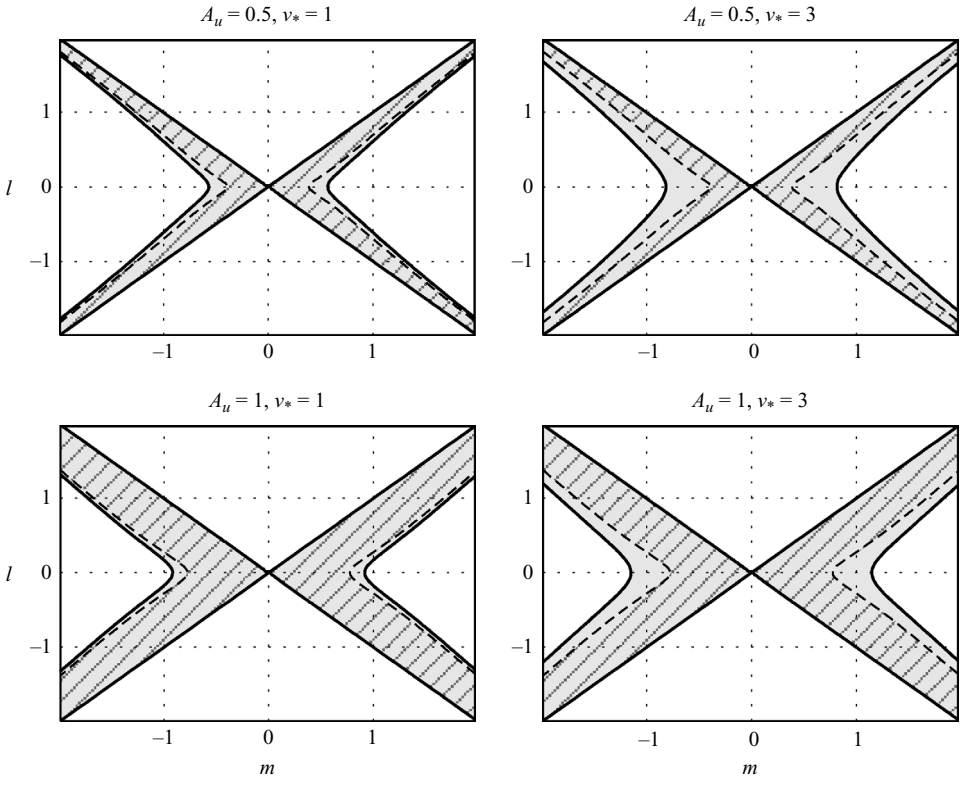

FIGURE 2. Shaded and bounded by solid lines: instability domains for several values of the carrier amplitudes A_u and friction, ν_*. Hatched and bounded by dashed lines: instability domains at $\nu_* = 0$. The water depth is $kh = 1.5$.

Similarly to (5.14), for instability to occur the term in curly brackets must be negative

$$D_{abs} = \mu\left(\mu + 2\alpha_\vartheta A_u^2 - \Lambda \tan\varphi\right) + \frac{2-\sigma}{(1-\sigma)^2}\,\Lambda^2 < 0. \tag{5.17}$$

Instability domains where (5.17) holds are shaded in figure 3. Solid lines enclosing the shaded region mark the position of the boundary, where $D_{abs} = 0$. For comparison the instability domains corresponding to the frictionless case are hatched and bounded by dashed lines. One can clearly observe that in terms of absolute perturbations the dissipation hampers development of instability and makes its domain to shrink in all cases. It is also worth noticing that it is the longitudinal perturbations that are most susceptible to the influence of friction. The observation that the longest perturbations are damped first might be important in the context of freak waves.

From a practical viewpoint, the most important issue is not whether modulations with a given wavevector will be unstable or not, but whether a wave field at hand can be stabilized by bottom friction and, if yes, what is the threshold value of the bottom roughness? A rough estimate of this value could be found immediately from (5.17) by requesting that the maximum of D_{abs} in the (m, l)-plane is exactly zero. For example, for purely longitudinal perturbations, $\mu = m^2$, $\alpha_\vartheta = \alpha_\parallel$, and the maximum of D_{abs} is attained when

$$\mu_+ = m_+^2 = \frac{\Lambda}{2}\,\tan\varphi - \alpha_\parallel A_u^2.$$

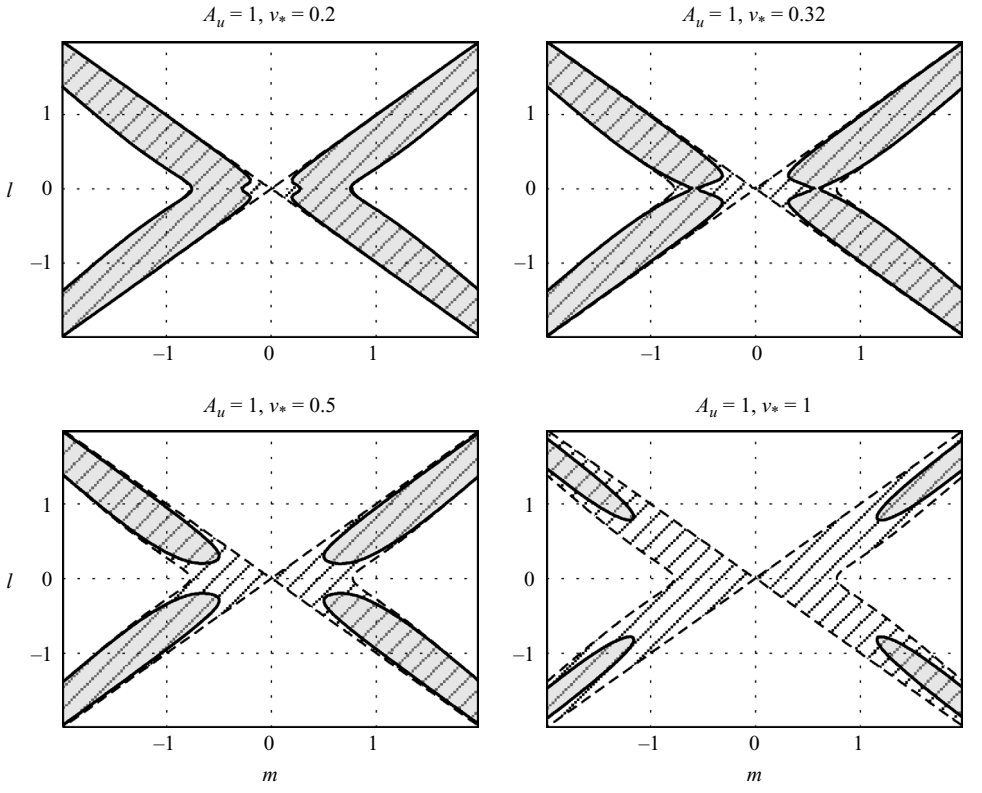

FIGURE 3. Shaded and bounded by solid lines: instability domains for several values of the carrier amplitudes A_u and friction, ν_*. Hatched and bounded by dashed lines: instability domains at $\nu_* = 0$. The water depth is $kh = 1.5$. Note that the values of parameters A_u and ν_* differ from those chosen for figure 2; in both cases the parameters were chosen to demonstrate most clearly the qualitative difference between the instability domains.

Substituting μ_+ into (5.17) we find that the perturbation with $m = m_+$ is neutrally stable (all other are damped), provided

$$\frac{2-\sigma}{(1-\sigma)^2}\,\Lambda^2 - \left(\frac{\Lambda}{2}\,\tan\varphi - \alpha_\parallel A_u^2\right)^2 = 0$$

or

$$\left\{\frac{(2-\sigma)^{1/2}}{1-\sigma} - \frac{\tan\varphi}{2}\right\}\,\Lambda = -\alpha_\parallel A_u^2. \tag{5.18}$$

Taking into account (5.4) and the fact that the instability only occurs at negative $\alpha_\parallel$, (5.18) can be further transformed to

$$\left\{(2-\sigma)^{1/2}\cos\varphi - \frac{1-\sigma}{2}\,\sin\varphi\right\}\,\frac{\nu_*}{|\alpha_\parallel|} = A_u^{1+\sigma}. \tag{5.19}$$

Taking $\varphi = 25^\circ$, $\sigma = 0.52$ the expression in the curly brackets is estimated to be very close to 1 and the criterion for longitudinal stability is

$$\frac{|\alpha_\parallel|}{\nu_*}\,A_u^{1+\sigma} \lesssim 1. \tag{5.20}$$

The expression on the left is simply the ratio of the magnitudes of the nonlinear and frictional terms in the NLS equation.

6. Formation of nonlinear patterns

Although the linear stability analysis performed in the previous section does shed some light on the influence of dissipation on the onset of modulational instability, it is not sufficient to understand the formation of nonlinear structures such as extreme waves. After a period of exponential growth, the amplitude of a sideband becomes finite, the linear approximation invalid and a full nonlinear model (4.18), or (4.19*b*), has to be considered. Fortunately, both the Davey–Stewartson and NLS equations are integrable as shown by Zakharov & Shabat (1971), and a number of exact nonlinear solutions were found to have simple analytical form. The most promising as prototypes of freak waves are solutions of a breather type, which may have amplitudes several times larger than the carrier wave and time spans of a few wave periods as pointed out by Henderson, Peregrine & Dold (1999) and Dysthe & Trulsen (1999). The former authors performed extensive numerical simulations of the propagation of a slightly modulated train of surface waves within the framework of full two-dimensional nonlinear Euler equations. They observed a number of 'steep wave events', bearing remarkable similarity to both ocean 'freak waves' and breather solutions of the NLS equation. Several types of breather solutions were found independently by Kuznetsov (1977), Kawata & Inoue (1978), Ma (1979), Akhmediev, Eleonskii & Kulagin (1987) and Peregrine (1983). The so-called Ma solitons are spatially localized and time-periodic, the Akhmediev breathers are periodic in space, but appear as a single event in time, whereas the Peregrine breather is aperiodic both in time and space. It is this last one that is the most promising as a good and simple analytical model of a prototype 'freak wave' event.

We hereinafter restrict ourselves to the (1+1) model. As the modulational instability is triggered at negative values of the coefficient $\alpha_\parallel$ only, take the complex conjugate and reduce (4.19*b*) to

$$\mathrm{i}\bar{A}_t + \bar{A}_{xx} + |\alpha_\parallel|\,|\bar{A}|^2\bar{A} + \mathrm{i}\nu_*\,\mathrm{e}^{-\mathrm{i}\varphi}\,|\bar{A}|^{1-\sigma}\,\bar{A} = 0. \tag{6.1}$$

Owing to the presence of a complex dissipation term no analytic solution is known at present and *a priori* a perturbation approach does not look particularly promising. Thus to study the effect of the bottom friction on the nonlinear development of the modulational instability and, in particular, breather formation, one has to resort to numerical simulations.

Rewrite (6.1) in the form

$$\bar{A}_t = \mathrm{i}\bar{A}_{xx} + \mathrm{i}F(\bar{A})\bar{A}, \tag{6.2a}$$

$$F(a) = |\alpha_\parallel||\bar{A}|^2 + \mathrm{i}\tilde{\nu}\,\mathrm{e}^{-\mathrm{i}\varphi}\,|\bar{A}|^{1-\sigma}, \tag{6.2b}$$

create grids in space and time

$$x_\jmath = \jmath\,\delta_x, \qquad t_n = n\,\delta_t, \tag{6.3a}$$

where

$$\jmath = -\frac{N}{2} : \frac{N}{2} - 1, \qquad \delta_x = \frac{2L}{N}, \tag{6.3b}$$

and impose periodic boundary conditions at the ends of the interval $[-L, L]$.

Starting from the initial condition in the form of a slightly modulated uniform wave

$$\bar{A}_J^0 = \bar{A}_0\{1 + \hat{a}\cos(m_r x_J)\}, \tag{6.4}$$

where $\bar{A}_u$, $\hat{a}$ are the initial amplitudes of the carrier and the sideband, the solution is advanced in time by using the split-step scheme of Besse (2004)

$$\Phi_J^{n+1/2} = 2F\left(\bar{A}_J^n\right) - \Phi_J^{n-1/2}, \tag{6.5a}$$

$$\frac{\bar{A}_J^{n+1} - \bar{A}_J^n}{\tau} = \mathrm{i}\mathbb{L}_h\left[\bar{A}_J^{n+1/2}\right] + \frac{\mathrm{i}}{4}\Phi_J^{n+1/2}(\bar{A}_{J+1} + \bar{A}_{J-1})^{n+1/2} \tag{6.5b}$$

$$\Phi_J^{-1/2} = F\left(\bar{A}_J^0\right). \tag{6.5c}$$

Here the subscript j marks the point on the spatial grid, the superscript n the number of the step in time. In this representation, $\mathbb{L}_h$ is the standard discrete operator of the second derivative

$$\mathbb{L}_h[\bar{A}_j]^n = \frac{\bar{A}_{J+1}^n - 2\bar{A}_J^n + \bar{A}_{J-1}^n}{\delta_x^2}, \tag{6.5d}$$

and the values at the intermediate moments of time $t_{n+1/2}$ are computed according to the rule

$$f^{n+1/2} = \frac{f^{n+1} + f^n}{2}. \tag{6.5e}$$

Spatial discretization is based on the integrable discrete NLS equation of Ablowitz & Ladik (1976). This has the advantage of being an exactly integrable discrete analogue of the continuous NLS equation, possessing a Hamiltonian structure, N exact conservation laws and other extremely useful properties. The most important one is that it does not induce a numerical chaos triggered by rounding errors (see Ablowitz & Herbst 1990). Breather solutions are homoclinic orbits of the NLS equation, i.e. they start and end in the vicinity of an unstable manifold (Mclaughlin & Shatah 1998). Proximity to homoclinic orbits can act as a source of chaos in weakly perturbed problems, and so numerical schemes based on the non-integrable spatial discretization of the NLS equation often exhibit irregular behaviour and are extremely sensitive to round-off errors.

The starting point for the development of instability ('fixed point') in the conservative case is the uniform solution

$$\bar{A}_c(x, t) = |\bar{A}_0|\exp(\mathrm{i}|\alpha_\parallel||\bar{A}_0|^2 t + \mathrm{i}\tilde{\phi}), \tag{6.6}$$

where A_0 is a constant and $\tilde{\phi} \in [0, 2\pi)$. In this sense there exists a ring of fixed points characterized by different values of the phase $\tilde{\phi}$, each of which can be a starting point for the development of homoclinic structure.

Assuming that the perturbation to (6.6) is harmonic in x, its period has to be a divider of the computational domain $2L$. Hence, only a countable number of modes is admissible, with wavenumbers given by

$$m_r = \frac{\pi r}{L},$$

where r is an integer. The growth rate, γ_r, of the rth mode is then given by

$$\gamma_{r\pm} = \pm m_r^2\left(\frac{2|\alpha_\parallel||\bar{A}_0|^2}{m_r^2} - 1\right)^{1/2} \tag{6.7}$$

and the mode is unstable when

$$0 < m_r^2 < 2|\alpha_\parallel||\bar{A}_0|^2. \tag{6.8}$$

The total number of admissible unstable modes is given by the largest integer M, satisfying

$$0 < M < (2|\alpha_\parallel|)^{1/2}\,\frac{|\bar{A}_0|L}{\pi}. \tag{6.9}$$

If M is larger than 1, several breathers of different periods may form simultaneously. Interactions between these breathers may result in a complicated structure of the wave field, which rapidly starts to resemble chaos. This homoclinic chaos is an inherent feature of the NLS equation and originates from coalescence of several homoclinic orbits, rather than from rounding errors or any other numerical inaccuracies (Ablowitz & Herbst 1990). Therefore, it cannot be avoided by error control, choice of discretization method or grid refinement.

A set of numerical computations has been performed at different values of the friction coefficient ν_* and the non-dimensional depth kh. The phase lag between the bottom stress and velocity in accordance with experimental data was taken to be $\varphi = 25°$. All runs started from the initial condition (6.4) with

$$\bar{A}_0 = 1, \quad \hat{a} = 10^{-3} \qquad \text{and} \quad M = 1 \tag{6.10}$$

The nonlinear coefficient $\alpha_\parallel$ is a function of non-dimensional depth kh only. Two values of the latter were chosen for simulations

$$kh = 1.5, \quad \Rightarrow \quad \alpha_\parallel = -0.2999 \tag{6.11a}$$

and

$$kh = 1.7, \quad \Rightarrow \quad \alpha_\parallel = -0.5923. \tag{6.11b}$$

The lengths of the interval in each case are

$$L = 7.5 \qquad \Rightarrow \qquad (2|\alpha_\parallel|)^{\frac{1}{2}}\,\frac{|\bar{A}_0|L}{\pi} \approx 1.895 \qquad \text{for} \qquad kh = 1.5 \tag{6.12a}$$

and

$$L = 5.5 \qquad \Rightarrow \qquad (2|\alpha_\parallel|)^{\frac{1}{2}}\,\frac{|\bar{A}_0|L}{\pi} \approx 1.938 \qquad \text{for} \qquad kh = 1.7, \tag{6.12b}$$

chosen to ensure that only one mode is unstable and to avoid the homoclinic chaos, as well as to maximize the amplitudes of the forming breathers.

Figure 4 shows one period of a pure Akhmediev's breather at $L = 7.5$, $kh = 1.5$. The uniform background solution $\bar{A}_u(t) = 1$ is subtracted for clarity. Akhmediev's breathers are a one-parameter family of solutions, so the choice of the period fixes the total maximal amplitude, $|\bar{A}_{max}| = 2.701$, in this case. This solution would certainly pass the amplitude criterion for a 'freak wave'. It is worth noting that the characteristic length of this solution specified by the width of the pulse at the level equal to twice the amplitude of the carrier is 1.4, which in non-scaled dimensional variables is $1.4\lambda/2\pi\varepsilon$, where λ is dimensional wavelength. For carrier steepness 0.1 the width is just $\sim 2\lambda$. The lifespan of the breather (defined as the period where $|A| > 2$) is 4, which for the same carrier steepness gives about 60 wave periods.

Figure 5 shows the result of calculations for $kh = 1.5$, $\nu_* = 0.025$. The uniform background solution, decaying in accordance with (5.6), is subtracted. The maximal relative amplitude of the perturbation is very small, $|\bar{A}_{max}| - \bar{A}_u = 0.109$, and taking

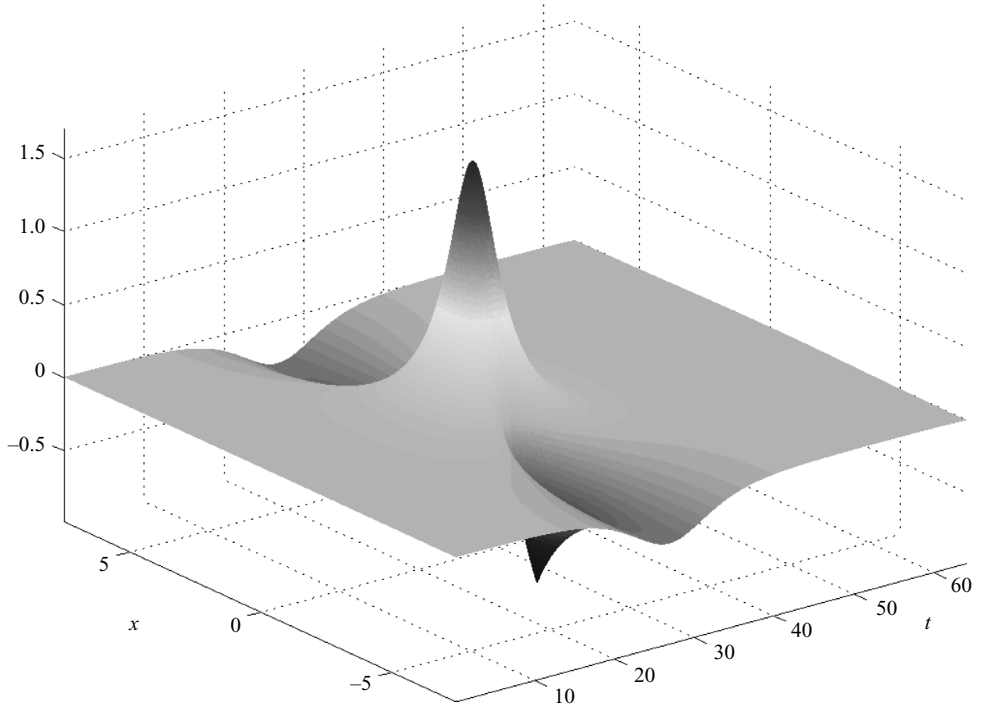

FIGURE 4. Pure Akhmediev's breather, $\nu_* = 0$, at $kh = 1.5$. The uniform background is subtracted.

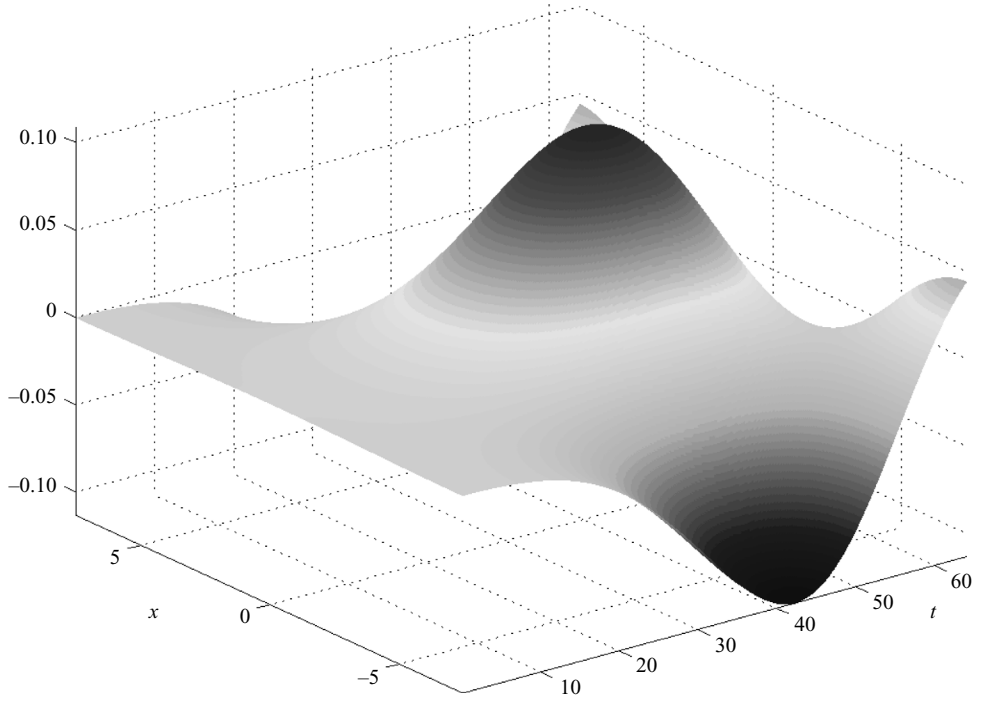

FIGURE 5. A breather damped by the bottom stress, $\nu_* = 0.025$, at $kh = 1.5$. The decaying uniform background is subtracted.

ν_*	0	0.005	0.01	0.015	0.02	0.025	0.03	0.35	0.04
$\max\{\lvert\bar{A}\rvert - \bar{A}_u\}$	1.699	1.366	1.025	0.669	0.315	0.109	0.045	0.023	0.014

TABLE 5. Maximal wave height vs magnitude of the friction at $kh = 1.5$. The decaying uniform background is subtracted.

ν_*	0	0.01	0.02	0.03	0.04	0.05	0.06
$\max\{\lvert\bar{A}\rvert - \bar{A}_u\}$	1.714	1.369	1.017	0.653	0.296	0.100	0.041

TABLE 6. As table 5 but at $kh = 1.7$.

into account that the background wave field is decaying, the observed total peak amplitude (background plus perturbation) does not exceed unity. Although technically the modulational instability still exists and manifests itself by the 10^2 growth of the initial 10^{-3} perturbation, this is, essentially, still a linear wave. From a practical viewpoint $\nu_{cr} = 0.025$ can be considered as a dissipative threshold for the onset of 'noticeable' modulational instability. The maximal amplitudes of the perturbation, $|\bar{A}_{max}| - \bar{A}_u$, obtained at different values of the friction coefficient are presented in table 5 for $kh = 1.5$ and in table 6 for $kh = 1.7$. At first glance the values of the friction coefficient, $\nu_{cr} = 0.025$ and $\nu_{cr} = 0.05$, could be taken as an effective threshold of the modulational instability at $kh = 1.5$ and $kh = 1.7$ respectively. Dissipation of this magnitude seems to prevent development of any noticeable modulational instability, i.e. the amplitude of the perturbation remains small and the envelope amplitude never exceeds the values typical for unperturbed linear waves. However, this is true only for the $O(10^{-3})$ or smaller initial perturbations. In contrast to the inviscid situation, the amplitude of the resulting breather is not predetermined but depends on the initial perturbation amplitude. Therefore a more robust criterion should be sought as the threshold for freak wave formation.

Roughly, one can assume that a freak wave does not form if, first, the relative amplitude of the perturbation never exceeds some pre-chosen finite value, $|\bar{A}_{max}| - \bar{A}_u < \bar{A}_{thr}$. We choose $\bar{A}_{thr} = 1$, which for example for the same initial amplitude (10^{-3}) results in

$$\left.\begin{aligned} \nu_{thr} &\simeq 0.01 \quad \text{at} \quad kh = 1.5, \\ \nu_{thr} &\simeq 0.02 \quad \text{at} \quad kh = 1.7. \end{aligned}\right\} \tag{6.13}$$

Second, we have to consider finite-amplitude initial perturbations and apply the already chosen maximal amplitude criterion. For example, for the initial amplitudes 0.01 and 0.1 the threshold values of friction ensuring that the perturbation (with the carrier wave subtracted) does not exceed 1 are, respectively, $\nu_* = 0.015$ and $\nu_* = 0.025$. Thus the friction required to stop freak wave formation depends on the initial amplitude of perturbations. It is worth emphasizing that the initial amplitude we are speaking about here relates only to the initial amplitude of a very special initial mode generating the breather, and not to the general level of broadband primordial noise typical of natural wave fields. The problem of relating the initial amplitude of this particular mode to the general noise level is in principle solvable under the assumption of *a priori* known noise distribution, but the noise distribution is not known. Instead we will attempt to guess the 'natural level' of noise by employing our numerical model. As we noted, in our setting the periodicity condition in space

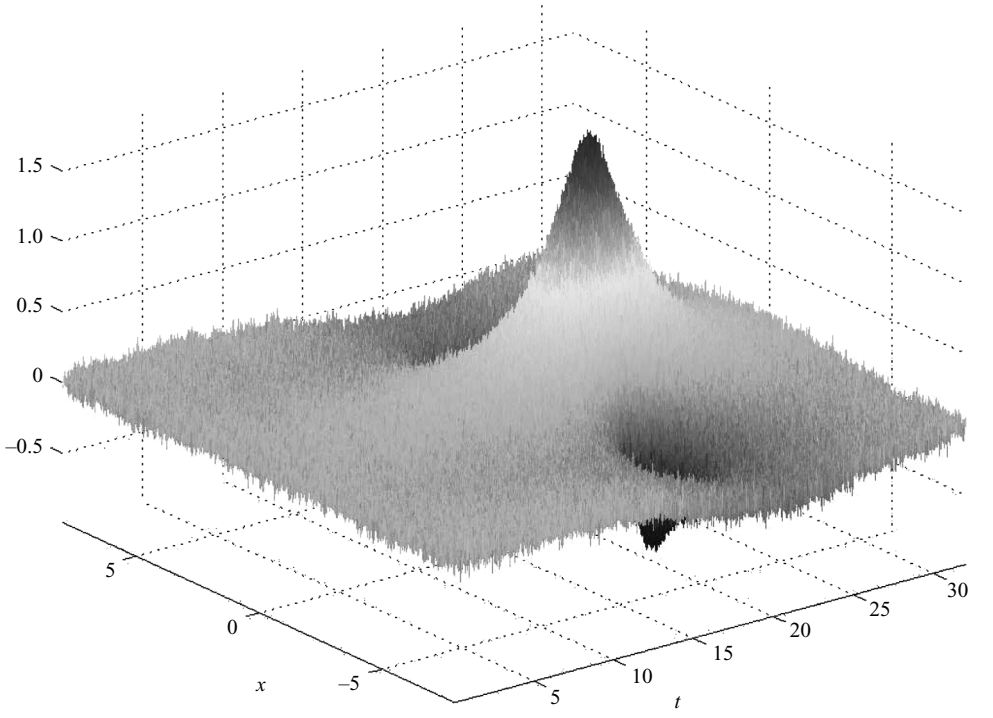

FIGURE 6. A 'fluffy' Akhmediev breather emerging out of initial white noise of amplitude 0.01, $\nu_* = 0$, at $kh = 1.5$. The uniform background is subtracted.

selects just a single mode which generates a breather. The presence of other modes does not noticeably affect the wave pattern as illustrated by figure 6 (cf figure 4) where an inviscid breather emerges out of a broadband (white) noise produced by 128 harmonics each having amplitude 0.01 and random phase.

The picture is not sensitive to the number of other modes either (simulations with 96 and 64 harmonics were also carried out). If we assume (we did not attempt two-dimensional simulations) that adding into the system another 128 transversal Fourier harmonics has a similarly negligible effect on the field evolution then we arrive at the situation where the integral energy contained in 10^4 modes of amplitude 10^{-2} is approximately equal to the energy of the basic wave. Therefore the initial amplitude level 10^{-2} might not be small and unrealistic. We stress that these values should be treated more like a guess than an estimate. We do not know what kind of mode selection occurs when no periodicity condition is imposed; the most likely outcome is some kind of homoclinic chaos. Even in the absence of friction the problem is not tractable by the Inverse Scattering Technique unless an artificial assumption of strong spatial localization of the initial noise is made. By choosing the initial amplitude of the breather mode to be one order of magnitude larger, i.e. 0.1, we probably strongly overestimate the natural noise level, but we guess that this would give us an estimate from above.

The frictional threshold for stemming freak wave formation based upon the above assumptions is much lower than that for the total suppression of modulational instability as the linear analysis (5.20) would suggest. There are two physical mechanisms at work, simultaneously responsible for this dramatic disparity. First, note that while the growth of perturbations slows down with amplitude, the friction

increases. This should halt the perturbation growth at a somewhat lower level. Second, friction leads to decay of the mean carrier wave amplitude as given by (5.6), which in itself results in significantly reduced maximal amplitudes attained by the growing perturbations. The relative importance of these two mechanisms is not clear. However, our preliminary simulations with the decay of the carrier wave amplitude artificially switched off seem to suggest that the second one is the main factor in the suppression of large-amplitude events.

It is also worth noting that the largest of the Akhmediev breathers and Ma solitons – the Peregrine soliton – corresponds in the inviscid limit to the longest initial perturbations which are more susceptible to bottom friction.

7. Discussion

The mathematical content of the study can be briefly summarized as follows. Employing a standard asymptotic technique, we derived an NLS-type evolution equation (4.18) for weakly nonlinear narrow-banded waves in water of finite depth, with the turbulent bottom stress taken into account. Under an appropriate scaling the bottom friction adds an additional dissipative term, $i\nu_* e^{i\varphi} |A|^{1-\sigma} A$, with all the specifics of the problem accumulated in the coefficient ν_* given by (4.18*c*). The bottom friction ν_* exceeding the critical value specified by (5.20) eliminates modulational instability, while $\nu_* > \nu_{thr}$ is sufficient to suppress the formation of breathers; ν_{thr} depends on the initial amplitude of the perturbations. The threshold values of $\nu_* = \nu_{thr}$ were found in the course of simulations relying upon questionable but explicit assumptions about the magnitudes of initial perturbations; the values of ν_{thr} proved to be surprisingly low, far less than 0.1 in all cases. However, the key question of how the model relates to the real world is much less clear, at the very least it requires a thorough discussion, which we attempt to provide below.

The point that is straightforward to clarify, is to convert to physical variables the model predictions made in terms of non-dimensional values of the friction coefficient ν_*. With the values of the exponent σ and the phase shift φ in the drag law (3.16*d*) fixed on the basis of experimental data (Soulsby *et al.* 1993), there remain four parameters determining the numerical value of ν_*: dimensional bottom roughness k_s, wavenumber $\mathscr{K}$ (or the wavelength $\lambda = 2\pi/\mathscr{K}$), wave steepness ε, and the non-dimensional depth kh. The main practical question this paper attempts to address can be formulated in several alternative ways.

Assuming the relative depth kh and the initial wave steepness ε are known, what roughness of the bottom is required to suppress a freak wave of a certain length?

An attempt to address this question is provided by figure 7. Each curve (a straight line in this case) in figrue 7(*a*) corresponds to the locus of the points in λ, k_s space where $\nu_* = \nu_{thr}$, the threshold value for freak wave (breather) formation based on the assumption of primordial noise of amplitude equal to 0.01. Different curves correspond to different values of steepness, ε, with the details provided by the legend. The waves of a given steepness subject to subthreshold modulations are above the corresponding curve. Similar results for $\nu_* = \nu_{thr}$ based on the 0.1 initial amplitude, which we believe provide an estimate from above, are shown in figure 7(*b*). The relative depth is fixed at $kh = 1.5$ in (*a*) and (*b*). The values of the bottom roughness in figure 7(*a*) are realistic: k_s is, normally, in the region of 1–30 cm as given for example by Grant, Williams & Glenn (1984), Myrhaug, Staatelid & Lambrakos (1998) or Lowe *et al.* (2005). However, the predictions shown in figure 7(*b*) based on the 0.1 initial amplitude suggest that to suppress freak waves of length λ exceeding

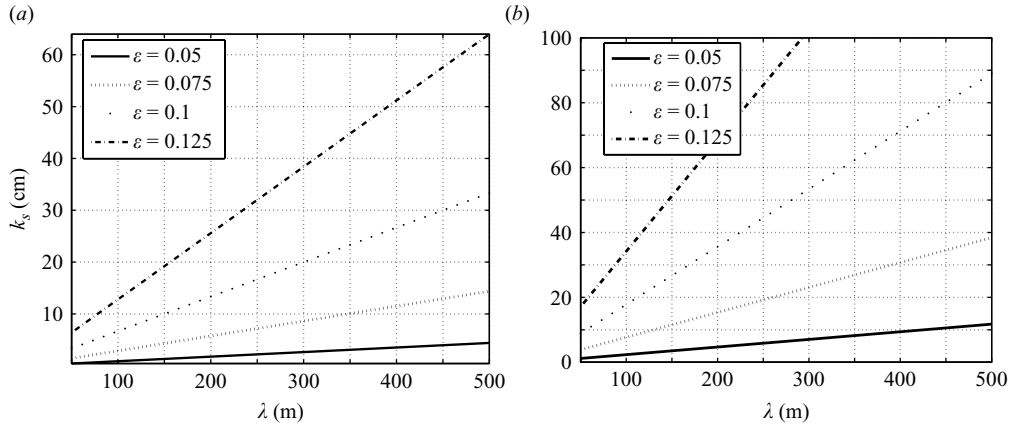

FIGURE 7. Wavelength/roughness-space diagram illustrating suppression of freak wave formation at $kh = 1.5$. (*a*) $\nu_* = \nu_{thr} = 0.015$, white noise (initial) amplitude is 0.01. (*b*) $\nu_* = \nu_{thr} = 0.025$, initial amplitude is 0.1. Formation of breathers exceeding the critical amplitude is suppressed above the corresponding curve.

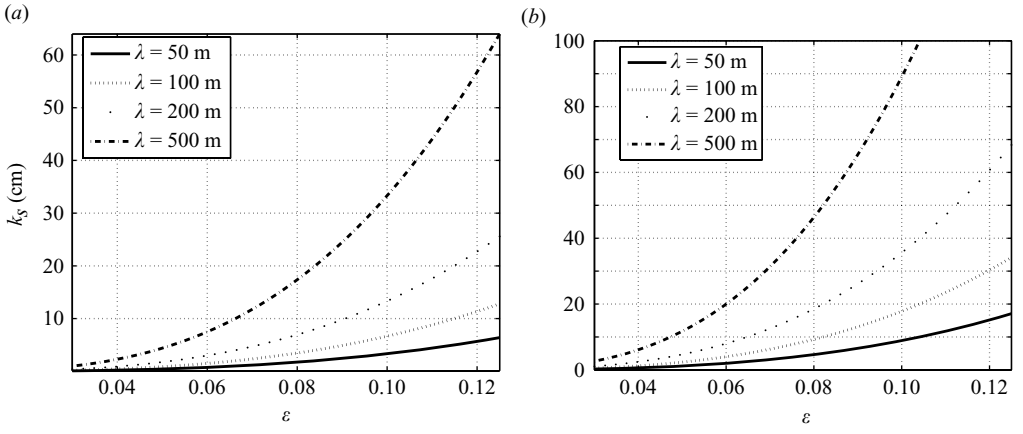

FIGURE 8. Steepness/roughness-space diagram of suppression of freak wave formation at $kh = 1.5$. (*a*) $\nu_* = \nu_{thr} = 0.015$, white noise (initial) amplitude is 0.01. (*b*) $\nu_* = \nu_{thr} = 0.025$, initial amplitude is 0.1. Formation of breathers exceeding the critical amplitude is suppressed above the corresponding curve.

250 m, and steeper than $\varepsilon \simeq 0.075$ a still realistic but much less common roughness ($k_s > 20$ cm) is required.

Assuming the relative depth kh and the wavelength λ to be known, what roughness of the bottom is required to suppress formation of a freak wave in a wave field of certain mean steepness/height? The answer to this question is suggested in figure 8. Each curve in figure 8(*a*) corresponds to the locus of the points in ε, k_s space where the friction coefficient is equal to ν_{thr}, the threshold value for freak wave (breather) formation calculated under the same assumptions as for figure 7(*a*). Different curves correspond to different values of the wavelength λ, with the details given in the legend. The waves of a given length are unlikely to exceed the critical amplitude in the domains above the corresponding curve. Similar results for $\nu_* = \nu_{thr}$ calculated

under the same assumptions as for figure 7(*b*), are shown in figure 8(*b*). Again the depth is fixed at $kh = 1.5$.

For example, for an ocean swell with $\lambda \simeq 500\,\mathrm{m}$ and $\varepsilon \simeq 0.05$, the threshold value of the bottom roughness required to prevent freak wave formation is about $k_s \simeq 4\,\mathrm{cm}$ (or $\simeq 12\,\mathrm{cm}$), depending on which of the two guesses about the level of initial noise is adopted. Typical wind waves are much shorter and steeper than the swell with $\lambda \simeq 50$–$100\,\mathrm{m}$, $\varepsilon \simeq 0.1$. Under the same assumptions similar estimates predict suppression of freak wind waves when roughness k_s exceeds 6 cm and 10–12 cm respectively.

However, the parameter to which the values of the dissipative threshold are most sensitive is the water depth, owing to both the growth of the nonlinear coefficient and primarily, the rapid decay of the orbital velocity, and hence bottom stress, with kh. The results of similar simulations at $kh = 1.7$ (not presented here) suggest that that the value of the bottom roughness required to prevent freak wave formation is generally unrealistic for sea conditions. The situation deteriorates rapidly with the growth of kh. The stabilizing influence of bottom stress is confined to water of depth

$$h' \lesssim \frac{1.5}{2\pi}\,\lambda \approx \lambda/4.$$

This yields $h' \lesssim 120\,\mathrm{m}$ for the swell, and $h' \lesssim 15$–$25\,\mathrm{m}$ for wind waves. It is worth reiterating that the range of interest of kh is not confined from below by the critical value $kh = 1.363$, but extends down to $kh \simeq 0.38$ for oblique modulations.

We would also like to emphasize that although we have focused our attention upon the range of depths which includes the critical (for longitudinal modulations) value $kh = 1.363$, in the suppression of the instability found, the vanishing of the cubic term coefficient $\alpha_{\|}$ at $kh = 1.363$ is not the main factor. The values of $\alpha_{\|}$ for $kh = 1.5, 1.7$ used in calculating the examples are finite (see (6.11)). The relative insignificance of this factor could be also seen from the fact of similar suppression of oblique instabilities considered in Appendix A and illustrated in figure 9 there.

The main physical implications of the model can be briefly summarized as follows. First, the bottom friction does affect evolution of surface waves in water of intermediate depth in a quite significant way. Apart from causing decay of mean height/steepness, it can suppress the wave modulational instability, especially its nonlinear stage. Surprisingly small values of the non-dimensional bottom stress prove to be enough to prevent weakly nonlinear prototypes of freak waves from reaching critical amplitudes. The threshold value depends primarily on the relative depth kh, on the bottom roughness, the incident wave length and steepness, and the key unknown–the natural level of low-frequency noise in the wave field. Estimates yield realistic values of bottom roughness, especially for ocean swell. Therefore, the effects described above are expected to be observable and the theory could be corroborated by data from the field in the future. At present, there are too few observations of freak waves; they are unique by their very nature, being an extreme event with a very low probability. At the same time, the decrease of mean amplitude is verifiable and can be checked by analysing available data.

The model proposed is a first approximation to the real world and it is appropriate to discuss its limitations, possible extensions and the ways of further developments.

We adopted *a priori* an $O(\varepsilon^3)$ scaling for the bottom stress. This (depending on wave steepness) seems to be most adequate for $kh \lesssim 1.3$, where only oblique instabilities could exist. Of course, such instabilities should be strongly suppressed by the friction even for a relatively smooth bed (see Appendix A). However, for the range of depths

$kh \simeq 1.5$–1.7, the estimates in § 3 suggest that the stress term might enter at the $O(\varepsilon^4)$ of the expansion (2.8) and still be of importance. At this order the finite width of the wave spectrum should be taken into account, leading to the next-order Dysthe-type generalization of the Davey–Stewartson or NLS equations for the envelope amplitude. Strictly speaking, it is the modification of such equations due to bottom stress (similar to the modification of the NLS already carried out and, crucially, with the same friction term) that should be studied to determine propensity of a wave field to 'freak wave' formation. For longitudional modulations the corresponding equation

$$\mathrm{i}A_t - A_{xx} + \alpha_{\|}|A|^2A + \{\beta A_{xxx} + \alpha_{21}|A|^2A_x + \alpha_{22}|A|^2\bar{A}_x\} + \mathrm{i}\nu_* \mathrm{e}^{\mathrm{i}\varphi}|A|^{1-\sigma}A = 0, \quad (7.1)$$

where ν_* is the same as in (4.18*c*), while the expressions for other coefficients valid for all depths can be found e.g. in Sedletsky (2003).

Yet we have chosen to remain within the framework of the modified NLS equation, since the main purpose of this paper is to demonstrate the existence of the effect and to develop the simplest possible model, rather than make detailed predictions which constitutes a subject for a separate study. Both the NLS and Dysthe-type equation (7.1) are derived for free water waves and their relevance for wind waves requires justification. Recall also that the time scales of envelope evolution within the framework of the NLS and Dysthe-type models are $O(\varepsilon^{-2})$ (apart from the $O(\varepsilon^{-3})$ supergroups in the Dysthe-type models). Direct wind forcing for spectral peak waves is negligibly small, while the 'indirect' wind input received by these waves via wind forcing of shorter waves and the inverse cascade is scaled at most as $O(\varepsilon^4)$ (e.g. Badulin *et al.* 2005). Thus, for both possible scalings of interest the modulation occurs at time scales much faster than those at which wind might affect the wave dynamics. Although the influence of the turbulent surface boundary layer on waves has not been studied in our context, the established view is that it is much weaker than that of the bottom boundary layer. In this sense, the total neglect of wind seems to be justified. One of the major implications of the fact that wind effects can appear only in higher orders is that the attenuation of the mean wave field predicted by our model cannot be balanced by wind input and, therefore, is not an artefact of the model.

The essence of the model and its fundamental limitation is the built-in assumption of weak wave nonlinearity. One may argue that a weakly nonlinear mechanism cannot create a highly nonlinear freak wave. Although this argument is difficult to dispute, we view the modulational instability as a necessary preliminary stage of freak wave formation, as was clearly shown by Dyachenko & Zakharov (2005) and Henderson *et al.* (1999). The situation is very similar to that in the problem of wave breaking: waves break via fast strongly nonlinear mechanisms as soon as the local slope exceeds 30° (Caulliez 2002). However, it is weakly nonlinear wave dynamics which determines whether and when the threshold is reached. Similarly, if the dissipation is strong enough to sufficiently suppress development of the modulational instability, it is also strong enough to make the emergence of freak waves via the modulational instability route impossible. It is obvious that the nonlinear friction, which increases with wave amplitude, also tends to inhibit formation of large-amplitude excursions of the wave field, whatever the underlying mechanism, although it is not clear to what extent freak wave formation caused by linear focusing is hampered by bottom fiction. With the modulational instability sufficiently suppressed we can only claim that the probability of a freak wave is somewhat less than that predicted by the Rayleigh distribution, which in itself has practical implications for offshore structure

design specifications. To get a quantitative estimate one has to undertake extensive direct numerical simulations within the framework of our model, which goes beyond the scope of the present paper. It is worth noting that as soon as the self-consistent nonlinear evolution of a random wave field is simulated within the framework of the model, then any assumptions on the level of noise are no longer needed. Only after such a study can intelligent decisions be made on where to locate an offshore structure and whether an artificial increase of roughness might be justified.

This work constitutes a part of the research contract 05/RFP/ENG085 from Science Foundation Ireland. Financial support of SFI is, hereby, gratefully acknowledged by V. V. V. and G. P. T. V. I. S. gratefully acknowledges support by INTAS through grant: 05-2206 8014.

Appendix A. Oblique modulations

Let us consider a plane wave modulation of the envelope oblique to the x-axis. That is, the amplitude of the envelope A and the induced pressure P in (4.18) are assumed to be functions of time and

$$\xi = x\cos\theta + y\cos\theta, \tag{A 1}$$

where θ is measured from the x-axis. Taking into account that

$$\frac{\partial}{\partial x} = \cos\theta\,\frac{\partial}{\partial \xi}, \qquad \frac{\partial}{\partial y} = \sin\theta\,\frac{\partial}{\partial \xi}, \tag{A 2}$$

equations (4.19) are transformed into

$$P_u = -\frac{\beta_p}{\eta} f_\theta\ |A_u|^2\,, \tag{A 3a}$$

$$\mathrm{i}A_t - \cos 2\theta A_{\xi\xi} + \alpha_\vartheta |A|^2 A + \mathrm{i}\nu_* \mathrm{e}^{\mathrm{i}\varphi}\,|A|^{1-\sigma} A = 0, \tag{A 3b}$$

where η, s, α_ϑ and f_θ are given by (4.16b), (5.2c).

Equation (A 3b) is self-focusing when $\alpha_\vartheta \cos 2\theta < 0$, even at $kh < 1.363$, provided the angle of incidence θ is different from zero. For example, in water of non-dimensional depth $kh = 0.7$, the BF instability of an oblique envelope is allowed for comparatively narrow range of angles $42^\circ \lesssim \theta \lesssim 45^\circ$. Choosing $\theta = 43^\circ$ implies $\alpha_\theta = -0.6104$ and the numerical simulations yield the following threshold values of friction for the same two cases: initial white noise of amplitude 0.01 and the breather mode of initial amplitude 0.1

$$\nu_{thr} = 0.015, \qquad \nu_{cr} = 0.025. \tag{A 4}$$

The diagrams in k_s, λ space in figure 9 outline the regions where the breathers originating from the particular class of initial conditions do not exceed two. The boundary is shown for several values of wave steepness ε given in the legend. Bottom roughnesses required to stop freak wave formation through the instability of oblique modulations of the wave envelope out of initial white noise of amplitude 0.01(left panel) are rather low: $k_s \lesssim 1$ cm. They are well below those typically occurring in nature. The values of k_s sufficient to prevent occurrence of breathers out of initial amplitude 0.1 are $k_s \lesssim 2$ cm which is at the low end of the values encountered in the sea. This suggests that the generation of freak waves at such depth is very unlikely, but one cannot exclude the arrival of a freak wave generated at larger depth.

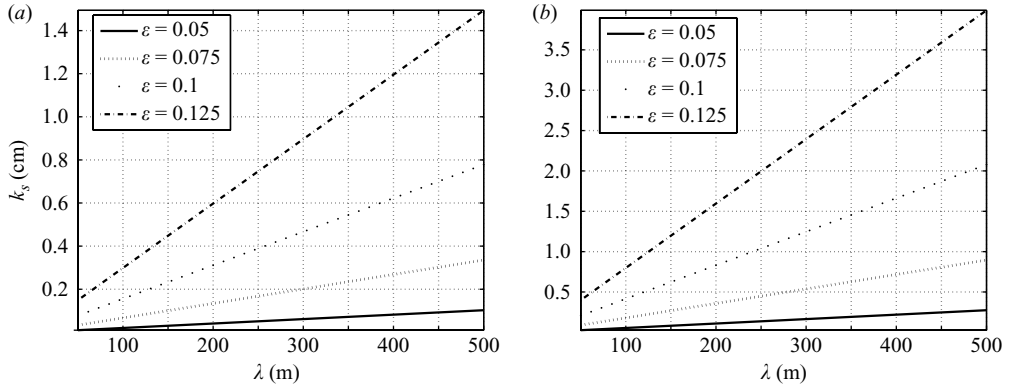

FIGURE 9. Steepness/roughness-space diagrams illustrating suppression of freak wave formation at $kh = 0.7$, $\theta = 43°$. (*a*) $\nu_* = \nu_{thr} = 0.015$, white noise (initial) amplitude is 0.01. (*b*) $\nu_* = \nu_{thr} = 0.025$, initial amplitude is 0.1. Formation of breathers exceeding the critical amplitude is suppressed above the corresponding curve.

Appendix B. Long-time asymptotics

The system (5.8) can be easily cast into a single equation

$$a_{tt} + \Lambda a_t + Da = 0, \tag{B 1}$$

which can be further transformed by the following change of the independent variable

$$\chi = \ln(1 + \Lambda_0 t) = \ln \frac{\Lambda_0}{\Lambda}, \quad \Rightarrow \quad \Lambda = \Lambda_0 \, \mathrm{e}^{-\chi}. \tag{B 2}$$

Consider

$$t \in [0; +\infty) \quad \rightarrow \quad \frac{\Lambda}{\Lambda_0} \in [1; 0) \quad \rightarrow \quad \chi \in [0; +\infty). \tag{B 3}$$

A new stability equations is

$$\tilde{a}_{\chi\chi} + \frac{\mu}{\Lambda^2}\left\{\mu + 2\alpha_\vartheta A_u^2 - \tan\varphi\Lambda\right\}\tilde{a} = 0. \tag{B 4}$$

No solution in closed form is known for the general version. However, (B 4) reduces to the Whittaker equation, provided

$$\frac{2\sigma}{1-\sigma} = 0; -1; -2, \quad \Rightarrow \quad \sigma = 0; -1.$$

Therefore, exact solutions in terms of the Whittaker functions are possible, if the friction coefficient in the quadratic drag law is

$$f_w = \text{const}, \quad \text{or} \quad f_w \sim A_u\,,$$

corresponding to the friction term being either quadratic or cubic in amplitude.

At large times, as $\chi \to +\infty$ and μ fixed, the first term in curly brackets in (B4) is dominant, and the equation is asymptotically close to

$$a_{\chi\chi} + \frac{\mu^2}{\Lambda_0^2}\,\mathrm{e}^{2\chi} a = 0,$$

the solution of which is

$$a = C_1 J_0\left(\frac{|\mu|}{\Lambda_0}\,\mathrm{e}^{\chi}\right) + C_2 I_0\left(\frac{|\mu|}{\Lambda_0}\,\mathrm{e}^{\chi}\right) = C_1 J_0\left(\frac{|\mu|}{\Lambda}\right) + C_2 I_0\left(\frac{|\mu|}{\Lambda}\right)$$

where $J_0(x)$, $I_0(x)$ are the usual Bessel functions. The amplitude of perturbation oscillates in time and slowly decays in absolute value

$$a \sim \frac{\sin\{|\mu|t + \theta\}}{\sqrt{|\mu|t}}, \qquad t \to \infty.$$

We have to point out, though, that this result is not of much practical value, since the long-time asymptotics are obtained on the basis of linear approximation. Nonlinearity will probably occur long before this stage is reached, unless the sideband is stable or close to the stability boundary from the very beginning.

REFERENCES

Ablowitz, M. J. & Herbst, B. M. 1990 On homoclinic structure and numerically induced chaos for the nonlinear Schrödinger equation. *SIAM J Appl. Maths* **50**, 339–351.

Ablowitz, M. J. & Ladik, J. F. 1976 A nonlinear difference scheme and inverse scattering. *Stud. Appl. Maths* **55**, 213–229.

Akhmediev, N. N., Eleonskii, V. M. & Kulagin, N. E. 1987 Exact first-order solutions of the nonlinear Schrödinger equation. *Theor. Math. Phys.* **72**, 809–818.

Badulin, S. I., Pushkarev, A. N., Resio, D. & Zakharov, V. E. 2005 Self-similarity of wind-driven seas. *Nonlin. Proc. Geophys.* **12**, 891–945.

Benney, D. J. & Roskes, G. J. 1969 Wave instabilities. *Stud. Appl. Maths* **48**, 377–385.

Besse, C. 2004 A relaxation scheme for the nonlinear Schrödinger equation. *SIAM J. Numer. Anal.* **42**, 934–952.

Caulliez, G. 2002 Self-similarity of near-breaking short gravity wind waves. *Phys. Fluids* **14**, 8, 2917–2920.

Colin, T., Dias, F. & Ghidaglia, J. M. 1995 On the rotational effects in the modulations of weakly nonlinear water waves over finite depth. *Eur. J. Mech.* B/*Fluids* **14**, 775–793.

Davey, A. & Stewartson, K. 1974 On three-dimensional packets of surface waves. *Proc. R. Soc. Lond.* A **338**, 101–110.

Djordjevic, V. D. & Redekopp, L. G. 1977 On two-dimensional packets of capillary-gravity waves. *J Fluid Mech.* **79**, 703–714.

Dyachenko, A. I. & Zakharov, V. E. 2005 Modulational instability of Stokes waves → freak wave. *JETP Lett.* **81**, 255–259.

Dysthe, K. B. & Trulsen, K. 1999 Note on breather type solutions of the NLS as models for freak-waves. *Phys. Scripta* T **82**, 48–52.

Grant, W. D. & Madsen, O. S. 1979 Combined wave and current interaction with a rough bottom. *J. Geophys. Res.* C **84**, 1797–1808.

Grant, W. D., Williams, A. J. & Glenn, S. M. 1984 Bottom stress estimates and their prediction on the Northern California continental shelf during CODE-1: The importance of wave-current interaction. *J. Phys. Oceanogr.* **14**, 506–526.

Hasegawa, A. & Tai, K. 1989 Effects of modulational instability on coherent transmission systems. *Opt. Lett.* **14**, 512–514.

Haver, S. 2000 On the existence of freak waves. In *Rogue Waves 2000* (ed. M. Olagnon & G. Athanassulis) IFREMEr, Brest, France. ISBN 2-84433-063-0.

Henderson, K. L., Peregrine, D. H. & Dold, J. W. 1999 Unsteady water wave modulations: fully nonlinear solutions and comparison with the nonlinear Schrödinger equation. *Wave Motion* **29**, 341–361.

Janssen, P. A. E. M. 2003 Nonlinear four-wave interactions and freak waves. *J. Phys. Oceanogr.* **33**, 863–884.

Janssen, P. A. E. M. 2004 *The Interaction of Ocean Waves and Wind*. Cambridge University Press.

Jensen, B. L., Sumer, B. M. & Fredsøe, J. 1989 Turbulent oscillatory boundary laters at high Reynolds numbers. *J. Fluid Mech.* **206**, 265–297.

Jonsson, I. G. 1980 A new approach to oscillatory rough turbulent boundary layers. *Ocean Engng* **7**, 109–152.

Kajiura, K. 1964 On the bottom friction in an oscillatory current. *Bull. Earthq. Res. Inst.* **42**, 147–174.

Kajiura, K. 1968 A model of the bottom boundary layer in water waves. *Bull. Earthq. Res. Inst.* **46**, 75–123.

Karlsson, M. 1995 Modulational instability in lossy optical fibers. *J. Opt. Soc. Am.* B **12**, 2071–2077.

Kawata, T. & Inoue, H. 1978 Inverse scattering method for the nonlinear evolution equations under nonvanishing conditions. *J. Phys. Soc. Japan* **44**, 1722–1729.

Kharif, C. & Pelinovsky, E. 2003 Physical mechanisms of the rogue wave phenomenon. *Eur. J. Fluid. Mech.* B/*Fluids* **22**, 603–634.

Klopman, G. 1994 Vertical structure of the flow due to waves and currents. *Progr. Rep. H 840, Part II*. Delft Hydraulics.

Komen, G. J., Cavaleri, L., Donelan, M., Hasselmann, K., Hasselmann, S. & Janssen, P. A. E. M. 1994 *Dynamics and Modelling of Ocean Waves*. Cambridge University Press.

Kuznetsov, E. A. 1977 On solitons in parametrically unstable plasma. *Dokl. USSR* **236**, 575–577 (in Russian) (English transl. *Sov. Phys. Dokl.* **22**, 9, 507–508).

Lamb, H. 1932 *Hydrodynamics*. Cambridge University Press.

Lowe, R. J., Falter, J. L., Bandet, M. D., Pawlak, G., Atkinson, M. J., Monismith, S. G. & Koseff, J. R. 2005 Spectral wave dissipation over a barrier reef. *J. Geophys. Res.* **110**, C04001.

Ma, Ya.-C. 1979 The perturbed plane-wave solutions of the cubic Schrödinger equation. *Stud. Appl. Maths* **60**, 43–58.

McLaughlin, D. W. & Shatah, J. 1998 Homoclinic orbits for pde's. In *Recent Advances in Partial Differential Equations, Venice 1996*. Proc. Symp. Appl. Maths, vol. 54, pp. 281–299. Am. Math. Soc., Providence, R.I.

Mei, C. C. & Hancock, M. J. 2003 Weakly nonlinear surface waves over a random seabed. *J. Fluid. Mech.* **475**, 247–268.

Mei, C. C. & Li, Y. 2004 Evolution of solitons over a randomly rough seabed. *Phys. Rev.* E **70**, 016302-1–11.

Mei, C. C. & Stiassnie, M. & Yue, D. K.-P. 2005 *Theory and Applications of Ocean Surface Waves*. World Scientific.

Myrhaug, D. 1989 A rational approach to wave friction coefficients for rough, smooth and transitional turbulent flow. *Coastal. Engng* **13**, 11–21.

Myrhaug, D., Staattelid, O. H. & Lambrakos, K. F. 1998 Seabed shear stresses under random waves: Predictions vs estimates from field measurements. *Ocean Engng* **25**, 907–916.

Nielsen, P. 1992 *Coastal Bottom Boundary Layers and Sediment Transport*. World Scientific.

Onorato, M., Osborne, A. R., Serio, M. & Bertone, S. 2001 Freak waves in random oceanic sea states. *Phys. Rev. Lett.* **86**, 5831–5834.

Osborne, A. R., Onorato, M. & Serio, M. 2000 The nonlinear dynamics of rogue waves and holes in deep-water gravity wave trains. *Phys. Lett.* A **275**, 386–393.

Peregrine, D. H. 1983 Water waves, nonlinear Schrödinger equations and their solutions. *J Austal. Math. Soc.* B **25**, 16–43.

Sedletsky, Yu. V. 2003 The fourth-order nonlinear Schrödinger equation for the envelope of Stokes waves on the surface of finite-depth fluid. *JETP* **97**, 180–193 (10.1134/1.1600810).

Segur, H., Henderson, D., Carter, J., Hammack, J., Li, G.-M., Pheiff, D. & Socha, K. 2005 Stabilizing the Benjamin-Feir instability. *J. Fluid Mech.* **539**, 229–271.

Sleath, J. F. A. 1987 Turbulent oscillatory flow over rough beds. *J. Fluid Mech.* **182**, 369–409.

Slunyaev, A., Kharif, C., Pelinovsky, E. & Talipova, T. 2002 Nonlinear wave focusing on water of finite depth. *Physica* D **173**, 77–96.

Smith, R. 1976 Giant waves. *J Fluid Mech.* **77**, 693–697.

Song, J.-B. & Banner, M. L. 2002 On determining the onset and strength of breaking for deep water waves. Part I: Unforced irrotational wave groups. *J. Phys. Oceanogr.* **32**, 2541–2558.

Soulsby, R. L. 1990 Tidal-current boundary layers. In *The Sea* (ed. B. Le Mehaute & D. M. Hanes). Ocean Engineering Science, vol. 9, pp. 523–566. Wiley-Interscience.

Soulsby, R. L. 1998 *Dynamics of Marine Sands*. Thomas Telford Ltd.

Soulsby, R. L., Hamm, L., Klopman, G., Myrhaug, D., Simons, R. R. & Thomas, G. P. 1993 Wave-current interactions within and outside the bottom boundary layer. *Coastal Engng* **21**, 41–69.

Swart, D. H. 1974 Offshore sediment transport and equilibrium beach profiles. Delft Hydraulics, Publ. 131.

Tanaka, M. 1990 Maximum amplitude of modulated wave train. *Wave Motion* **12**, 559–568.

Terray, E. A., Donelan, M. A., Agrawal, Y. C., Drennan, W. M., Kahma, K. K., Hwang, P. A. & Kitaigorodskii, S. A. 1996 Estimates of kinetic energy under breaking waves. *J. Phys. Oceanogr.* **26**, 792–807.

Thais, L., Chapalain, G., Simons, R. R., Klopman, G. & Thomas, G. P. 2001 Estimates of decay rates in the presence of turbulent currents. *Appl. Ocean Res.* **23**, 125–137.

Zakharov, V. E. 1968 Stability of periodic waves of finite amplitude on the surface of deep water. *J. Appl. Mech. Tech. Phys.* **9**, 190–194.

Zakharov, V. E. & Shabat, A. B. 1971 Exact theory of two-dimensional self-focusing and one-dimensional self-modulation of waves in nonlinear media. *Zh. Eksp. Teor. Fiz.* **61**, 118–134.